Universidad de Valladolid

ESCUELA DE INGENIERÍAS INDUSTRIALES

UNIVERSITY OF VALLADOLID

SCHOOL OF INDUSTRIAL ENGINEERINGS

Master in chemical Engineering

MASTER THESIS

Oxidation of sugar mixtures on gold nanoparticle extrudates

Author:

HERRERO MANZANO, MARIA

Supervisor:

GARCIA SERNA, JUAN , SALMI, TAPIO

ÅBO AKADEMI

Valladolid, Julio 2020.

TFM REALIZADO EN PROGRAMA DE INTERCAMBIO

TÍTULO: Oxidation of sugar mixtures on gold nanoparticle extrudates

ALUMNO: María Herrero Manzano

FECHA: Fecha de la defensa en la universidad de destino

CENTRO: ÅBO AKADEMI UNIVERSITY

TUTOR: Tapio Salmi, Juan García Serna

INDEX

FIGURE INDEX

LIST OF SYMBOLS

Glu	Glucose	θ_i	Coverage at the catalyst surface
Ara	Arabinose	ε_p	Particle porosity
GluO	Gluconic acid	ρ_p	Particle density
GluRO	Glucoronic acid	s	Shape factor
AraO	Arabinonic acid	R	Gas constant
Fruc	Fructose	D	Molecular diffusion coefficient
Rib	Ribulose	D_{ei}	Efective diffusion coefficient
Ci	Concentration inside the particle	X	Association factor
C'i	Concentration in the bulk phase	M	Molar mass
Pi	Partial pressure	$\tilde{V}$	Molar volume
Ni	Amount of substance	μ	Viscosity
ri	Reaction rate	τ	Tortuosity
K	Kinetic constant		

KEYWORDS

Oxidation of sugars, biomass valorization, heterogeneous catalysis, gold catalyst

ABSTRACT

The current work was carried out at the Laboratory of Industrial Chemistry and Reaction Engineering, Department of Chemical Engineering at Åbo Akademi University (Turku/Åbo, Finland) in collaboration with University of Valladolid within the framework of Erasmus mobility. The supervisors were Academy Professor Tapio Salmi and Professor Dmitry Murzin from the host university and Professor Juan García Serna from the home university.

The project was focused on the valorization of biomass from forest-based feedstock. The aim was the catalytic oxidation of sugar mixtures on gold nanoparticles supported on alumina. The sugars, originating from biomass hydrolysis, can be valorized by oxidation of a hydroxyl group to a carboxyl group, giving the corresponding sugar acid. These sugar acids are useful for the alimentary, pharmaceutical and construction industry as additives.

Nowadays, alternative feedstock and more sustainable technologies are continuously under development and research, avoiding the use of oil feedstock in future. Green chemistry and green process technology are the areas of chemical engineering focusing on the design of products and processes, which minimize the environmental impact. Biorefinery belongs to this concept concerning the biomass conversion starting with non-petroleum feedstock and developing more sustainable processes.

During this work, several experiments were conducted in a laboratory-scale semi-batch reactor at 70^{o}C, pH 8 and atmospheric pressure. The system was equipped with a titrator, which automatically added sodium hydroxide into the reaction mixture to maintain a constant alkaline pH. The oxidation of two C5 and C6 sugars, arabinose and glucose, on gold nano-particles were studied in this project. One of the novelties of this oxidation process is the application of SpinChemTm technology, which allows the use of immobilized catalyst and high turbulence to suppress external mass transfer limitations around the catalyst particles and giving the opportunity to study the reaction in a middle step between discontinuous and continuous processes. Liquid-phase samples were withdrawn from the reaction mixture during the experiments and the samples were analyzed by high-performance liquid chromatography (HPLC). A catalyst synthesized in the laboratory and a commercial one were used in the kinetic experiments. Both catalysts were characterized with transmission electron microscopy (TEM), scanning electron microscopy (SEM), nitrogen physisorption and particle size analysis.

Catalyst deactivation was observed in successive experiments with recycled catalyst extrudates. It was confirmed by ICP-MS that the reason for the deactivation was leaching. Moreover, the kinetic results revealed strong internal mass transfer limitation in the pores of the catalyst extrudates. A mathematical model was derived for the reaction kinetics and the parameters in the model were estimated by non-linear regression analysis. Further studies are needed to completely understand the chemistry of the system and to implement continuous reactor technology. Even new catalyst without gold content could be screened.

SPANISH ABSTRACT - RESUMEN

El presente trabajo fue realizado en el laboratorio de química industrial e ingeniería de la reacción en Åbo Akademi University (Turku, Finlandia) con la colaboración de la Universidad de Valladolid (Valladolid, España) en posesión de una beca de movilidad Erasmus. El trabajo fue supervisado por Tapio Salmi, Dmitry Murzin y Juan García Serna.

El proyecto enfocado en la revalorización de la biomasa proveniente de residuos forestales tiene como objetivo el estudio de la reacción de oxidación de azucares sobre un catalizador con nano partículas de oro. Los azucares, provenientes de la hidrólisis de la biomasa, pueden ser revalorizados mediante la fijación de un átomo de oxígeno en un grupo hidroxilo originando un grupo carboxilo en la molécula. Los azúcares ácidos obtenidos son compuestos de valor añadido usados en la industria farmacéutica, alimentaria y de la construcción como aditivos. El creciente desarrollo de nuestra sociedad ha obligado a la industria a buscar nuevas fuentes de materias primas, alternativas al petróleo y más sostenibles.

Es por ello que la investigación está orientada al progreso de procesos eficientes y sostenibles, procesos que favorezcan el desarrollo sostenible como la teoría "Green chemistry". Dentro de esta teoría encontramos conceptos como el aplicado en este proyecto, el concepto de biorrefinería. El concepto de biorrefinería hace referencia al conjunto de procesos y tecnologías que convierten la biomasa en energía y productos de valor añadido.

Durante el desarrollo de este proyecto se llevaron a cabo experimentos en un reactor semi-batch a 70^{o}C, pH 8 y presión atmosférica equipado con un sistema de adicción automática de hidróxido sódico que permitía controlar de una forma precisa el pH. La reacción de oxidación de dos azúcares básicos C5 y C6 (arabinosa y glucosa respectivamente) gracias a la presencia de nanopartículas de oro sobre alúmina que actuaban como catalizador. El sistema disponía de una tecnología nueva conocida como SpinChemTM que permite tener inmovilizado el catalizador dentro de una red que favorece el flujo de fluido desde la parte inferior de la cesta a las paredes exteriores de ella. El dispositivo funciona a su vez como agitador, proporcionando un buen mezclado que permite depreciar las limitaciones de transferencia de materia externa. Este dispositivo es un paso intermedio entre el reactor discontinuo y continuo, dando una idea de cómo sería la reacción teniendo en cuenta la difusión de los reactivos y los productos en la superficie del catalizador. Las muestras fueron tomadas manualmente y analizadas en una columna de cromatografía líquida de alta eficacia. Se sintetizó un catalizador y se testó un catalizador comercial, ambos fueron caracterizados usando métodos de análisis como TEM, SEM, N_2 physisorption y Malvern análisis.

Se observó una clara desactivación del catalizador aparentemente debido a la lixiviación sufrida por la pérdida de oro en la fase líquida. Además de un alto efecto de la transferencia de materia interna. Futuros estudios son necesarios para la completa comprensión de este sistema y su desarrollo en un reactor continuo. Igualmente, una nueva propuesta de catalizador, sin contenido en oro, surgió durante el desarrollo del proyecto, la cual necesita ser estudiada en profundidad.

ACKNOWLEDGMENT

I would like to express my special gratitude to my professors Tapio Salmi and Juan García Serna as well as professor Dmitry Murzin for allowing me to carry out this project on the topic oxidation of sugar mixtures which helped me a lot in developing research skills and professional knowledge.

I sincerely thank my friends, family members and old college mates who provided me the help I needed to carry out this labour, taking advantage of the knowledge and hard skills for making my project as best as I can.

I am very fortunate for all the help given by the laboratory manager docent Kari Eränen in practical matters during my experimental work as well as docent Narendra Kumar and associate professor Päivi Mäki-Arvela, for supporting me during TEM analysis.

I am very grateful for all the help people at the Laboratory of Industrial Chemistry and Reaction Engineering gave me. Especially, I would like to thank Sebastian who tutored me in the first steps of the work, Zuzana for the patience she dedicated to me elaborating the extrudate catalyst, Adriana who helped me a lot during the development of the project and everybody who has directly or indirectly collaborated with me in this task.

1. INTRODUCTION

Climate change is one of the most severe challenges of our society. The current dependence of the mankind on fossil fuels has serious consequences for our planet. That is why there is a growing interest to promote sustainable development. Alternative technological solutions and different feedstock should be promoted. The concepts of green chemistry and green process technology are used to design new chemical processes on a more sustainable basis, using renewable raw material and supressing the generation of hazardous and harmful components. The concept of green chemistry is based on 12 principles including design, feedstock, synthesis, processes, energy, application, and impact. One of the implementations of the green chemistry principles is the biorefinery concept [1].

The concept of biorefinery focuses on developing new and more sustainable processes and products. It comprises all the processes, new technologies, and equipment to produce bioenergy and bio-products from renewable carbon resources. There is a huge diversification in biorefinery feedstock including for instance, lignocelluloses, algae, and waste materials.

Earth generates 1.3 billion tons per year of biomass while just 3% is consumed by man. In Europe, the availability of biomass is limited, so technological improvements are needed in order to create a flexible and efficient industry of the future [2]. Biomass can be treated by gasification to synthesis gas or by low temperature processes, such as hydrolysis of cellulose and hemicelluloses to sugars. Following these two lines, molecules in biomass can be converted into fuels, chemicals, materials heat, and power.

Lignocellulosic biomass consists of lignin (15-30%) [3], cellulose (40-60% in weight) [4], and hemicelluloses (15-30% in weight) [5], so mostly it is composed by carbohydrates. Cellulose and hemicelluloses are both polysaccharides made up of sugar monomers. Cellulose is a straight-chain polymer formed by β-glucose monomers while hemicelluloses are branched polymers consisting of several monomers of pentoses and hexoses. By controlled hydrolysis of hemicelluloses under mild conditions, aldoses are obtained which can be oxidized to sugar acids. This work is focused on the oxidation of five-carbon and six-carbon sugars, arabinose and glucose. Gluconic acid and arabinonic acid are the main products[6,7].

Gluconic acid and arabinonic acid have several applications, for instance, they are used as additives in pharmaceutical, alimentary, and cosmetic industries. Moreover, the conjugate base of gluconic acid, gluconate, along with many minerals are applied in medical injections and cleaning products [8,9]. There are recent investigations about the chelating properties of gluconic acid to extract rare earth metals under mild pH conditions instead of using sulfuric acid [10].

1.1. THEORETICAL BASIS

1.1.1. Glucose and arabinose

Carbohydrates can be considered the most abundant natural molecules, and they are present in various chemical and biochemical processes, from plant photosynthesis to energy supply in cells.

Carbohydrates are composed of carbon and water following the formula $C_x(H_2O)_y$. Most of them are aldoses or ketose. Figure 1 shows the Fischer projection formulae for acyclic D-aldoses [11].

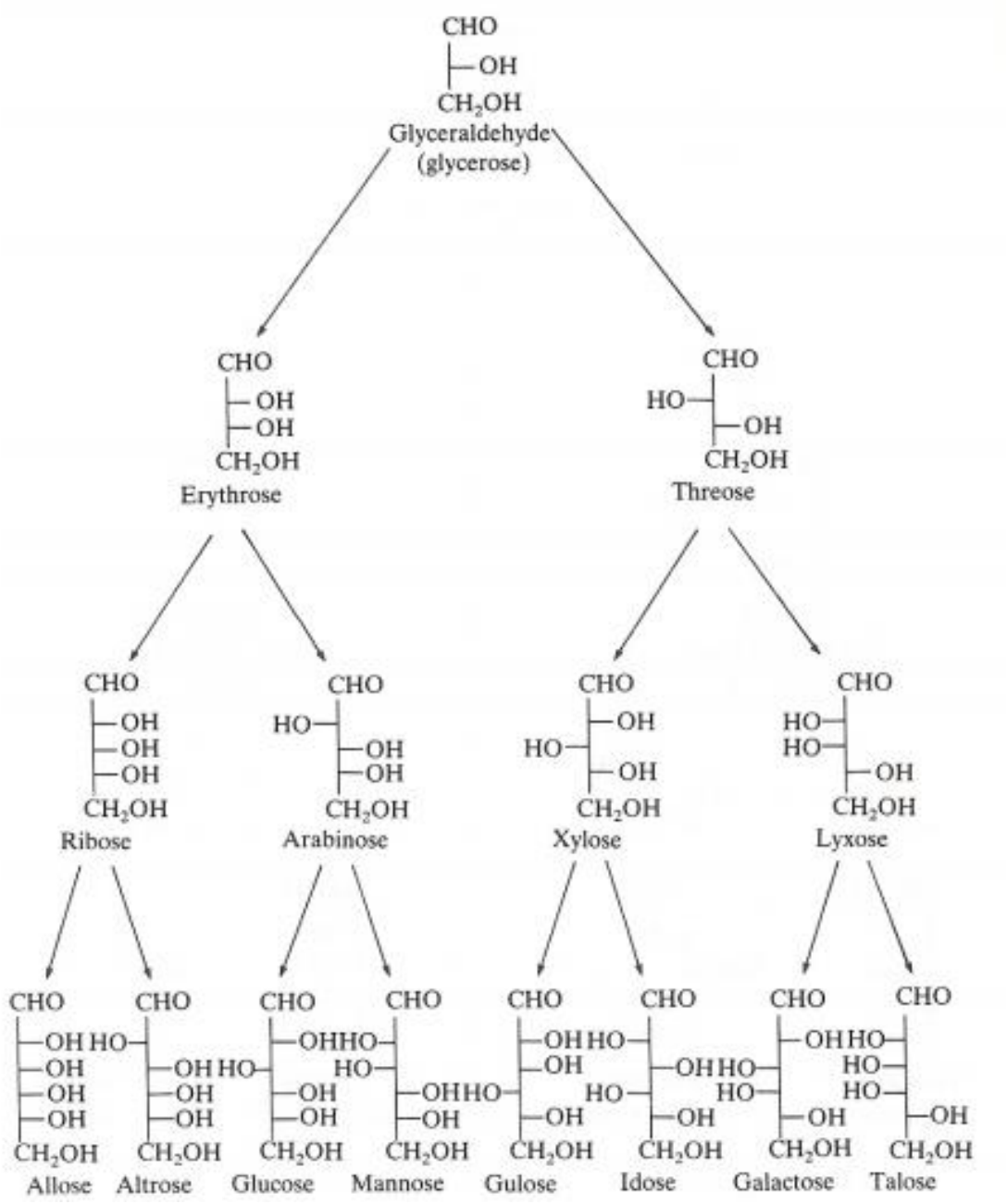

Figure 1:Family of D- Aldoses.

For a carbohydrate system with "n" chiral carbon atoms, there are 2^n stereoisomers, composed by 2^{n-1} enantiomers (mirror image). According to the theory of van't Hoff, glucose would have four carbons chains. Thus, there exists 16 isomers of which 8 are enantiomers. As the glucose used in this project is D-glucose which has the hydroxyl group on the right-hand side of the lowest carbon chain. The forms of the D-glucose can be summarized as 8 enantiomers [12,13].

An alkaline solution with pH > 10 promotes the aldose-ketose isomerization of glucose to fructose but at a higher pH it promotes the formation of mannose. Fructose is a D-ketose formed when aldehyde group change the position with the hydroxyl group on the lowest chain carbon.

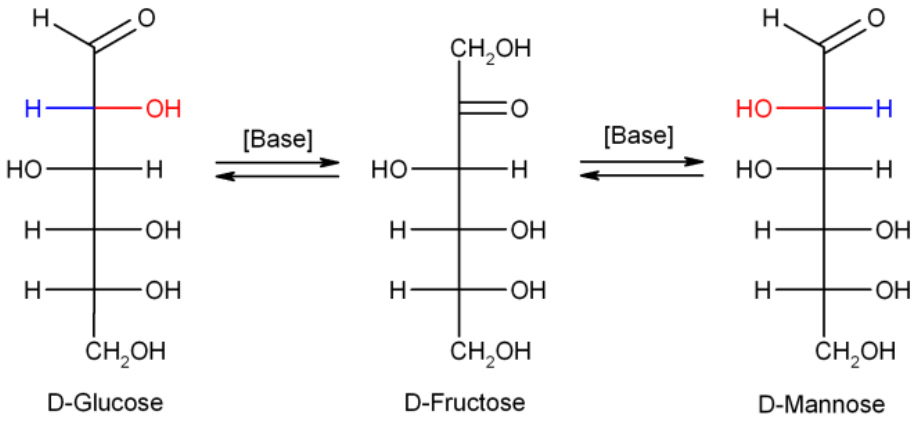

Figure 2 : Glucose Isomerization.

Glucose is an aldohexose, a six-carbon sugar with an aldehyde group or a cyclic hemiacetal functional group. It co-exists as straight-chain and ring forms. The dissolution of sugars results in an equilibrium between different optical rotation forms of the substance, called mutarotation.

The open form of glucose appears less than 0.02% in aqueous solutions. More than 99% of glucose exists in the form of pyranose. Pyranose is a six-membered carbon cycle including an oxygen atom in the ring. Sometimes, there is a five-membered carbon cycle ring known as furanose which exists in lower concentrations in the solution. This ring undergoes mutarotation at carbon-1, which is the anomeric carbon. There are two anomers known at 112° and 19° of rotation, called α-D-glucopyranose and β-D-glucopyranose for the pyranose form and α-D-glucofuranose and β-D-glucofuranose for the furanose form [13,14].

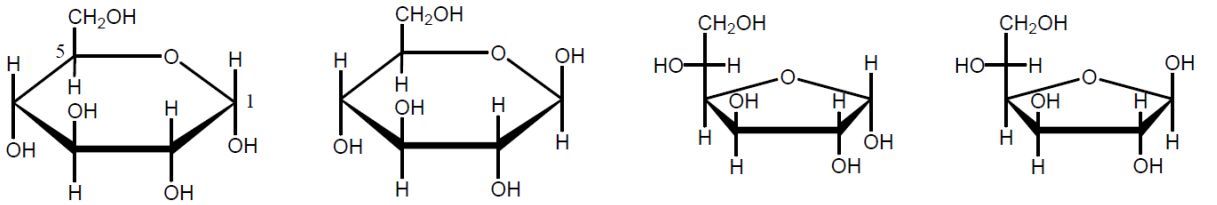

α-D-glucopyranose β-D-glucopyranose α-D-glucofuranose β-D-glucofuranose

Figure 3: Cyclic forms of glucose.

A similar theory can be applied for L-arabinose, giving five cyclic compounds, α-L-arabinopyranose and β-L-arabinopyranose, α-L-arabinofuranose and β-L-arabinofuranose [15], as well as ribulose from the aldose-ketose isomerization of arabinose. These isomers of glucose and arabinose has been confirmed previously in the presence of heterogeneous catalysts such a gold on carbon in alkaline environment [16].

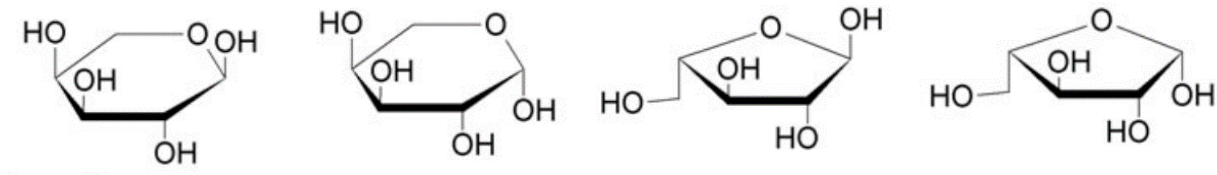

α-L-Arabinopyranose β-L-Arabinopyranose α-L-Arabinofuranose β-L-Arabinofuranose

Figure 4: Cyclic forms of arabinose.

1.1.2. Reaction mechanism of sugar oxidation

Sugar acids are obtained by oxidation of the hydroxyl group in the original sugar. Aldoses can be oxidazed to aldonic acid whereas, ketoses are resistant for oxidation.

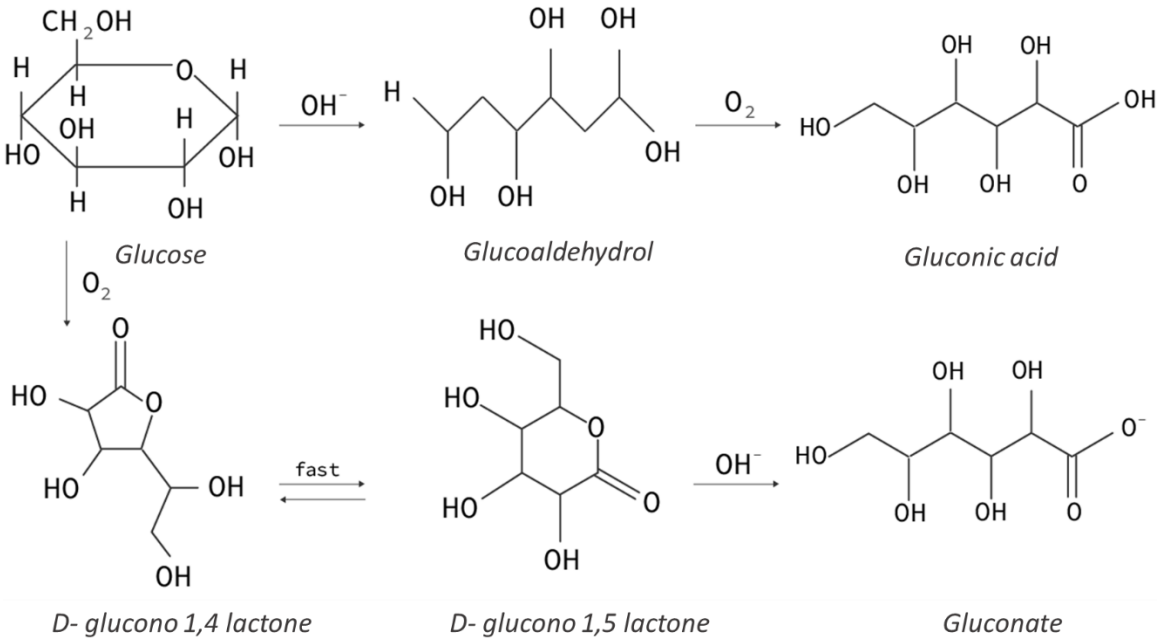

Figure 5: Glucose oxidation [17].

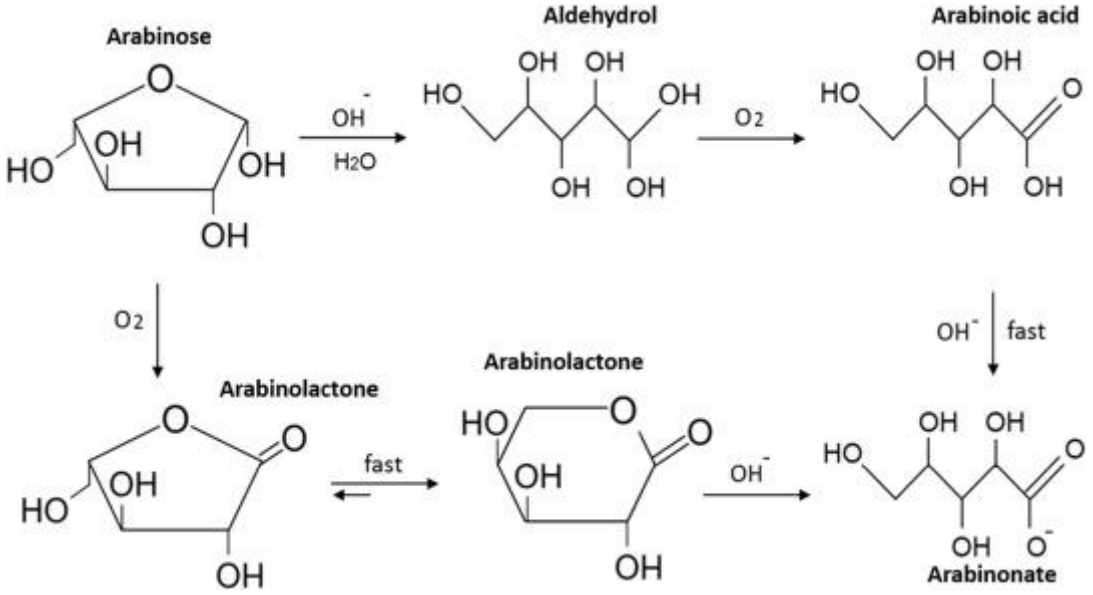

Figure 6: Arabinose oxidation [18].

The oxidation takes place in two stages. Firstly, on the metal surface area the dehydration of the hydroxyl group takes place, resulting in the creation of the corresponding lactone, which is the rate determining step. Secondly, oxygen is reduced releasing an oxygen atom which joins the lactone giving the sugar acid form. This oxygen originates from the oxygen feed due to the dependence of the rate on the partial pressure of oxygen instead of the oxygen from the water dissociation. From the work of Kusema et al [19] and the shift of the potential on

the surface area, one can presume a plausible reaction mechanism by measuring the protons and electrons absorbed on the surface area of the catalyst. In the beginning of the process the aldose is absorbed on the catalyst surface following by dissociative absorption of oxygen at the edges, the dehydrogenation to the lactone occurs at the faces, thus oxygen migrates to the faces in order to react with the lactone giving the corresponding sugar acid.

It can be assumed that glucose and arabinose follow a similar pattern, in addition gluconolactone and arabinolactone appear as intermediate compounds.

1.1.3. Catalyst

A catalyst is a substance that increases the reaction rate but it does not become consumed in the reaction. The presence of the catalyst in a chemical process promotes a different reaction pathway under milder conditions. Enzymatic and heterogeneous catalytic processes have been applied for the oxidation of sugars. The heterogeneous catalytic process is performed mainly with molecular oxygen in an aqueous medium on a noble metal catalyst such as palladium, platinum or gold [20].

Noble metal catalysts, such as palladium, platinum and gold, are particularly efficient in the oxidation of carbohydrates having a high activity and selectivity to the corresponding sugar acids at mild temperatures [21,22]. Indeed, gold catalyst has clear benefits compared to other noble metals. During the reaction, some metals can be poisoned by the oxygen losing the activity while gold catalyst does not show this behaviour [23]. The activity and selectivity of gold are related to the number of defect sites on the surface area of the nanoparticles and the interface between the gold particles and the support. The best conditions are found in nanoparticles with diameters around 2 nm [19].

Catalyst supports with an oxygen content demonstrated a higher catalytic activity than the ones without oxygen [24]. Moreover, previous research has shown higher rates with alumina support than carbon support, probably because gold particles on carbon support are larger which is unfavourable for the oxidation process.

The catalyst used in this work had 1 weight % gold loading of nanoparticles around 2 nm. Two different catalysts were applied in the oxidation process, a powder catalyst that was synthesized at the Laboratory of Industrial Chemistry and Reaction Engineering, and commercial extrudates obtained from Strem Chemicals.

2. OBJECTIVES

The aim of this work is to determine the oxidation kinetics of selected sugar mixtures, specifically, glucose and arabinose to obtain added-value compounds such as arabinonic acid or gluconic acid.

Previous studies have been conducted in batch reactors using different kinds of powder catalysts, but in future we shall move forward to understand how gold catalysts will work in a continuous reactor. A continuous process has several advantages compared with batch and semi-batch processes. For a continuous process, automation is easier and cleaning of the reactor system is needed, usually, just once per year. Continuous reactors are very suited for large-scale production because production stops are not needed between the batches. Moreover, the reaction product obtained from a continuous process is more uniform than from a discontinuous process.

To achieve this goal, a novel mixing technology known as SpinchemTM was used in this work. This new technology allows the use of immobilized catalyst extrudates in a batch reactor to get similar results to those which might be obtained with a continuous reactor. Moreover, the Spinchem device enhances mass transfer, suppressing external mass transfer limitations and improving the contact between the liquid and gas phases [25]. Before changing to a continuous process, the catalyst which will be used for the continuous process should be selected. Thus the activity, selectivity and durability of the immobilized catalyst will be screened to predict the potential of a continuous reactor technology in order to shift to continuous operation in a future work.

3. PLAN

Previous work carried out at the Laboratory of Industrial Chemistry and Reaction Engineering at Åbo Akademi was focused on the kinetic modelling of sugar oxidation [26], performing the reaction with a finely dispersed powder catalyst to minimize mass transfer limitations to reveal the intrinsic kinetics on the catalyst surface. The current work is devoted to catalyst extrudates to study the interaction of intrinsic kinetics and mass transfer effects.

The catalyst was used in the same shape as it would have been used in a continuous reactor. The data were analysed to understand the liquid and gas internal mass transfer coupled to the oxidation kinetics on the catalyst surface.

4. EXPERIMENTAL SECTION

4.1. Catalyst

4.1.1. Laboratory prepared catalyst

Gold was deposited on alumina via the precipitation-deposition method using hydrogen tetrachloroaurate(III) hydrate (99.9%-Au) (49% Au) (chloroauric acid) (Alfa Aesar and ABCR GmbH) as the precursor. It is the most common way to prepare alumina supported gold catalysts.

Temperature, pH, precursor concentration, alumina pre-treatment, calcination and washing, are important parameters to control the features of the catalyst. Some of them, such as pH have a strong influence on the gold loading, the dispersion of gold nanoparticles and the cluster size [27].

The catalyst preparation process was performed at 70^{o}C, increasing the pH gradually until it reached pH 8 because the precipitation of Au is related to the existence of neutral species. Once the desired pH was achieved, the reaction was continued at constant temperature and pH for three hours.

After completing the reaction, the catalyst was washed with distilled water and filtered to remove chlorine species. Finally, the material was dried out overnight at 100^{o}C and the calcination was continued for six hours at maximum 300^{o}C.

4.1.2. Extrusion efforts

In order to use the Spinchem device for kinetic experiments, the powder catalyst should be transformed into extrudates. The first attempt was to use fresh alumina to analyse the extrusion results with this material which had not been tried before for this kind of equipment.

After a sieving pre-treatment, the slurry was shaped with fresh alumina, water, and some organic compounds of high molecular weight working as a glue, following by drying and calcination steps before performing the extrusion.

Several slurry mixtures were screened and different percentages of Bindzil binder (colloidal silica Bindzil-50/80 (50% SiO2 in water, Akzo Nobel) added. The proportion of these components is extremely important for the extrusion, otherwise, the slurry can be too dry or too wet for the extrusion. The obtained extrudates can lose the catalytic activity if the amount of Bindzil is too high, but a low percentage of it can result on weak extrudates which cannot have enough strength to be used in a reactor. After diverse experiments along a month, using different composition for the slurry, even 50% Bindzil, the results were unsuccessful.

4.1.3. Commercial catalyst

We also tested gold (1%) on aluminum oxide extrudates (AUROlite™ Au/Al_2O_3) in kinetic experiments. These dark purple extrudates might have been useful for catalytic oxidation. They have a size of 1.2mm x 5mm and the gold nanoparticles are around 2-3 nm, which is an optimal cluster size for many applications. These extrudates were supplied by Strem Chemicals, a manufacturing company specialized in high purity chemicals for scientific research and development.

Actually most of the catalyst extrudes were broken and did not keep the original measurements. From a measurement test of some of the fresh extrudates the average diameter was 1 mm and the average length between 2 and 4 mm, presenting some exceptions in which the extrudates were up to 8 mm long.

4.1.4. Characterization

4.1.4.1. Particle size

The macroscopic particle size distribution of a solid catalyst is an important physical property, understanding how it affects the overall reaction rate and mass transfer in the particles. Malvern analysis is a laser diffraction equipment used for evaluating the particle size of a solid sample. The particle size distribution was analysed by an equipment provided by Malvern Instruments Ltd.

4.1.4.2. TEM

Transmission electron microscopy (TEM) gives the distributions of metal nanoparticles on catalyst support. TEM was performed with a suspension of the gold catalyst on ethanol. A beam of electrons is conducted to a catalyst sample, which is suspended on a grid giving a nanoscale image of the catalyst. This method provides high resolution images from which the amount and the size distribution of the nanoparticles on the support can be determined.

4.1.4.3. ICP

Inductively coupled plasma mass spectrometry (ICP-MS) is used to analyse the amounts of metals in liquid and solid samples. This technique was applied to determine the precise amount of gold in our catalysts. The sample of the solid catalyst was dissolved completely in an acid mixture consisting of nitric acid and hydrochloric acid. The fresh catalyst was analysed giving a total loading of 1.3% of gold content.

4.2. Sugar mixture oxidation

4.2.1. Experimental setup

The experimental work was carried out in an isothermal laboratory-scale semi-batch reactor fully equipped. The reactor set-up is shown in Figure 7. At first glance, it is a transparent glass reactor with 250 ml of capacity. The temperature was controlled by a heating/cooling jacket using distilled water. The temperature and pH were measured by an automatic system controlled by a 907 Titrando device. This device, delivered by Metrohm, adds automatically the base or acid to control the pH during the experiment. As the reaction products are acids, addition of an alkaline solution is needed for the control pH. For the experiments described in this project, sodium hydroxide solutions with concentrations from 0.2 M to 1.0 M were used, depending on the reaction time of each experiment.

Stirring was performed by a propeller head made from stainless steel under which it is located the Spinchem device. The catalyst and plastic spheres to avoid breaking the catalyst during the reaction time were placed inside this device. This new technology combines the benefits of batch and continuous processes because the catalyst is immobilized in the pellet shape but operated in a batch reactor. The results give an idea about how the catalyst might work in a continuous system. Moreover, the Spinchem supresses external mass transfer limitations in the liquid phase, because high turbulence prevails around the particles.

The sugar solution was filled at the reactor while the oxygen-nitrogen mixture flow was continuously added by a Brooks 5850S mass flow control device. The reactor had a safety gas outlet which maintained the total pressure constant at 1 atm and the reactor was combined with a cooling system connected to a water line. In this way, completely isothermal conditions were preserved.

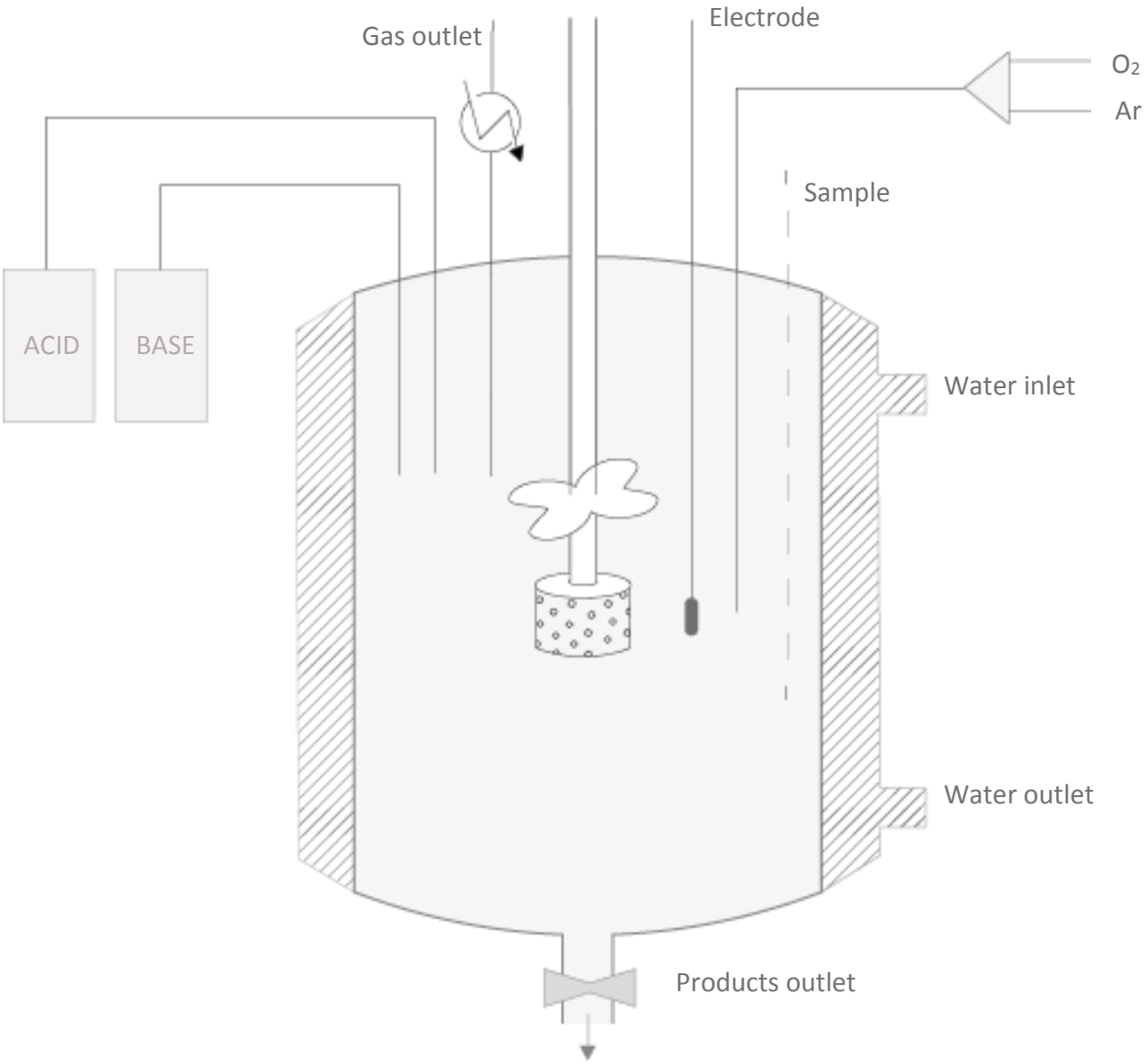

Figure 7: Reactor Set up.

4.2.2. Kinetic experiments.

Different procedures were applied because both powder and extrudate catalysts were used, but the general idea was the same. The sugar mixture solution of L-arabinose (Sigma-Aldrich, ≥99%) and anhydrous D-glucose (Fluka, ≥98%) was prepared in a 150 ml beaker and heated until the desired reaction temperature (70^{o}C) was reached. The mixture was added to the reactor under an inert atmosphere previously created by flushing with argon. The powder

catalyst was added to the reactor before the solution when the reactor was at inert atmosphere and appropriate temperature while extrudates were placed in the Spinchem basket. The Spinchem device was filled with 1 g of the catalyst and 1 mm diameter plastic balls which immobilized the catalyst particles and prevented breaks.

The pre-heated reactor was kept at 73^{o}C when the sugar solution was added to the reactor. Under a well-controlled pH and temperature, the solution remained inside the reactor until the pH and temperature were constant. At this moment, a mixture of 5 ml/min of oxygen and 35 ml/min of argon was fed into the reactor vessel. The stirring speed was kept between 900-1000 rpm to reduce the mass transfer limitations. The pH was controlled with Titrando equipment which added NaOH automatically. The concentration of the NaOH solution was different depending whether the reaction was performed with catalyst powder or extrudates. The extrudate catalyst showed very low rates in comparison with the powder catalyst mainly because of internal mass transfer limitations. Thus, a small droplet of NaOH generates a big impact on the reaction while the reaction rates are low. Consequently, 1M NaOH was used for the powder catalyst and 0.2 M NaOH for the extrudates.

The sampling was done by using a syringe and withdrawing a sample of around 1 mL from the reaction mixture. In both cases, for powder catalysts and extrudates, a 0.45 µm PVDF filter was used to remove any catalyst from the samples.

5. RESULTS AND DISCUSSION

5.1. Sugar oxidation

The experiments were performed both with the catalyst powder and the extrudates. The powder catalyst was used to understand the reaction and test the activity of the catalyst. Moreover, the diffusion phenomena should show lower rates with an increasing catalyst particle size. Therefore, some experiments with crushed catalysts were conducted to analyse the dependence between the reaction rate and the particle size.

Secondly, the investigation was focused on the oxidation study in the presence of diffusion limitations. Experimental parameters such as temperature and pH have been researched previously concluding that the optimal operation point is at 70^{o}C, pH 8 and oxygen partial pressure 0.125 atm. The amount of commercial catalyst available was limited so the deactivation experiments were carried out preferentially, followed by the experiments with different initial molar ratios of the sugars. One of the characteristics of the project is the

oxidation of sugar mixtures wherefore knowing the preferential oxidation pathway is an important issue.

5.1.1. Powder catalyst

5.1.1.1. Diffusion phenomena

To investigate the existence of diffusion limitations inside the catalyst pores, various experiments using different catalyst particle sizes were compared. The experiments were carried out under identical conditions: 70ºC, pH 8, 1:1 sugar mass ratio, 0.125 oxygen partial pressure, and higher than 900 rpm stirring speed. The particle size of the catalyst was measured by Malvern analysis. Four experiments are compared in this section:

- The reaction by powder catalyst. The particle size of the powder is below 65 µm.
- The reaction by crushed catalyst small size. 90 % of the particles are above 371 µm.
- The reaction by crushed catalyst big size. 90 % of the particles are above 732 µm.
- The reaction by extrudates, using the Spinchem rotating basket reactor.

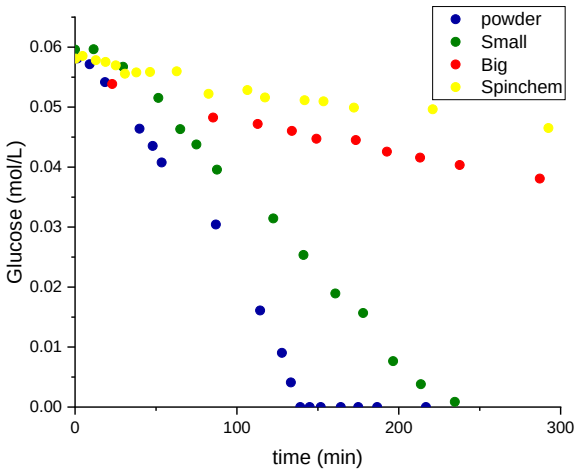

Figure 8: Glucose consumption at different catalyst sizes.

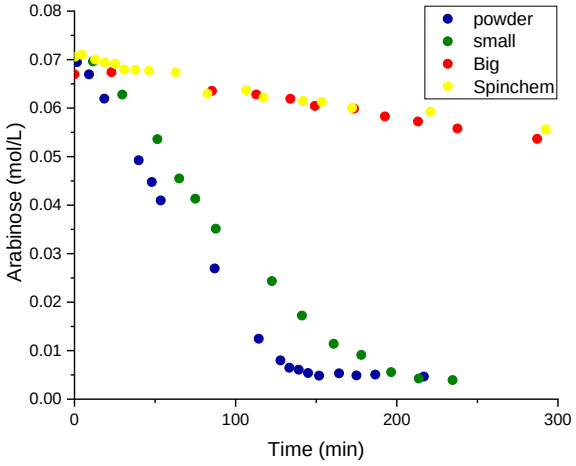

Figure 9: Arabinose consumption at different catalyst sizes.

Both plots in Figures 8 and 9 show a clear decreasing rate with an increasing particle size, which suggests the existence of mass transfer limitation phenomena; this limitation might be mainly caused by internal mass transfer. External mass transfer limitations are negligible due to the high stirring speed. Thus, it can be assumed that the oxidation is limited by internal mass transfer in the pores of the catalyst extrudate.

The results from de Malvern Analysis of each crushed catalyst can be found in Appendix I.

5.1.2. Catalyst extrudates

As the results showed a clear internal mass transfer limitation, the reaction times were studied at first place to adequate the system for the reaction with the extrudates. The reaction times were increased from three hours (around 100% conversion) with the powder catalyst to more than three days with the extrudates. Consequently, the Titrando system was adjusted, using a lower concentration of the NaOH solution. Some molar concentrations of NaOH were tried, concluding 0.2 M of NaOH provided a stable control of the pH along the reaction, instead of 1.0 M, which was used for the powder form of the catalyst.

The limited amount of catalyst available (10 g of catalyst) and the time limitation due long reaction times implied that certain experiments are given priority over others. Firstly, it was crucial to analyse the possibility of reusing the catalyst doing deactivation experiments. Secondly, the main study should be focused on the oxidation of the sugar mixtures, trying to understand which is the preferential pathway of oxidation.

5.1.2.1. Catalyst deactivation

To measure the catalyst deactivation, three different experiments using the same recycled particles inside the Spinchem device were carried out. The reaction was performed at 70^{o}C, pH 8, oxygen partial pressure 0.125 atm, stirring speed exceeding 900 rpm, 1:1 molar ratio of arabinose-to-glucose and 1 g of catalyst. Between the experiments, the system was washed several times with deionized water keeping on the heater and the stirrer to ensure proper cleaning. After each experiment, the reactor was filled with argon to maintain an inert atmosphere.

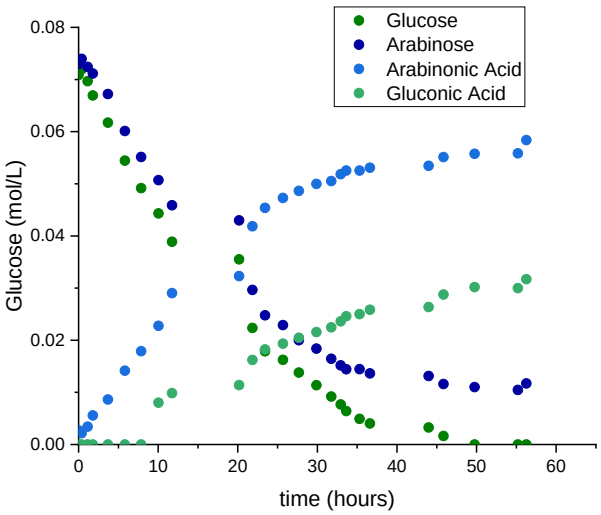

Figure 10: 1st use of the catalyst on sugar oxidation

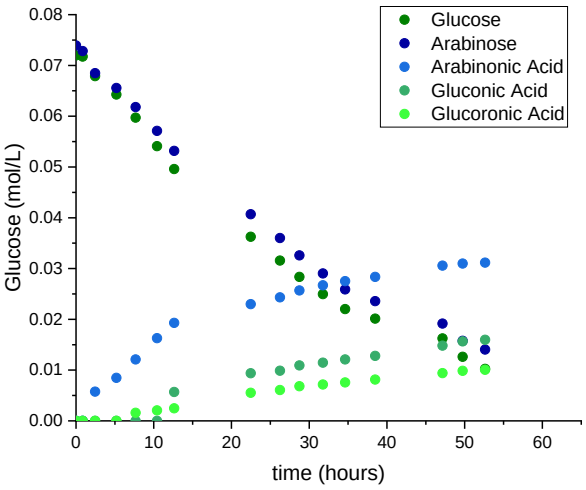

Figure 11: 2nd use of the catalyst on sugar oxidation

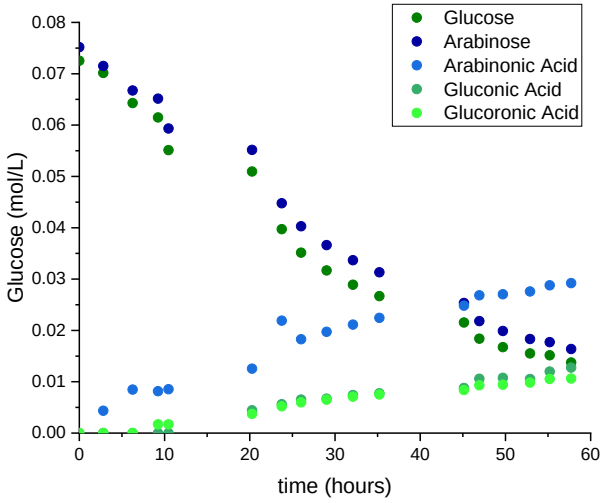

Figure 12: 3rd use of the catalyst on sugar oxidation

Figures 10-12 confirm a clear catalyst deactivation in each experiment. Not only the rate but also the selectivity of the reaction changed from cycle to cycle. While in the first use, the main products were arabinonic acid and gluconic acid, in the following ones the amount of glucoronic acid produced is increased. Figure 13 shows the comparison of the glucose consumption in every experiment. Some studies reports that leaching of gold is important a pH 7, thus it will be necessary to carry out further research to solve this issue [28].

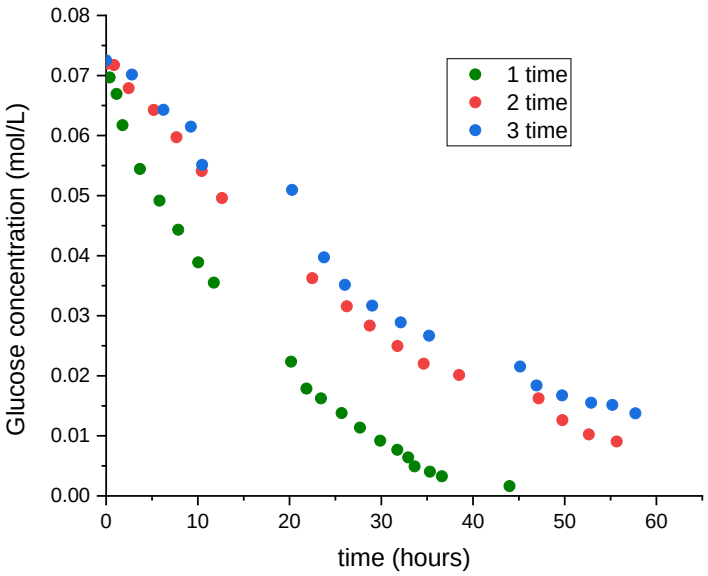

Figure 13: Glucose consumption at 3 times used.

The deactivation can be studied with some catalyst characterization methods. To check the possible leaching of gold into the liquid phase, three samples; fresh catalyst, once used catalyst and triple used catalyst were analysed with ICP-MS. The results are shown here:

Sample	Wt%
Fresh	0.86
Spent 1	0.82
Spent 3	0.75

The results suggest that the gold content is dissolved into the aqueous phase, the catalyst is deactivated. Leaching of catalyst is an irreversible phenomenon leading to the disappearance of active sites from the surfaces of heterogeneous catalysts operating in liquid phase. Many new processes in biorefineries use this kind of catalysts, which makes the issue very crucial [29].

5.1.2.2. Molar ratio of sugars

The experiments with different initial molar ratios were conducted in order to check which sugar is preferentially oxidized arabinose or glucose. The reference conditions were the 1:1 molar ratio glucose-to-arabinose at pH 8, 70^{o}C, stirring speed <900 rpm and 1 g of catalyst. Two additional experiments were performed changing the molar ratio glucose-to-arabinose to 2:1 and 1:2 under similar conditions. The results are displayed in Figures 14-16.

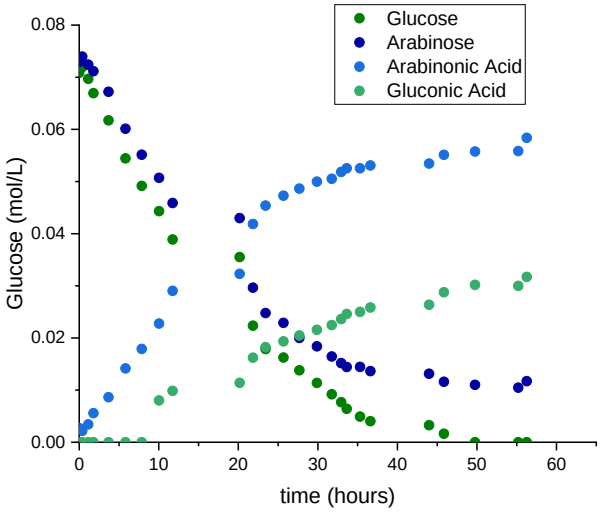

Figure 14: 1G:1A molar ratio.

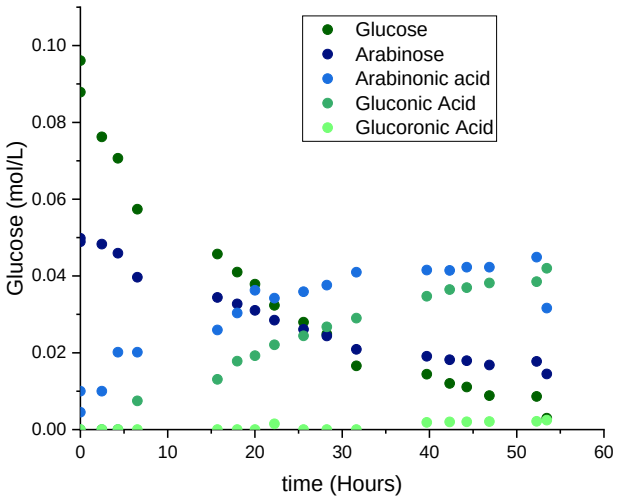

Figure 15: 2G:1A molar ratio.

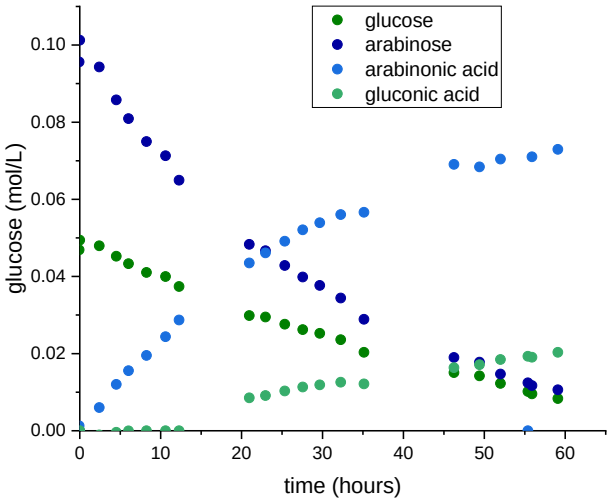

Figure 16: 1G:2A molar ratio.

Checking the mass balance for each experiment:

- 1 Arabinose: 1 Glucose molar ratio

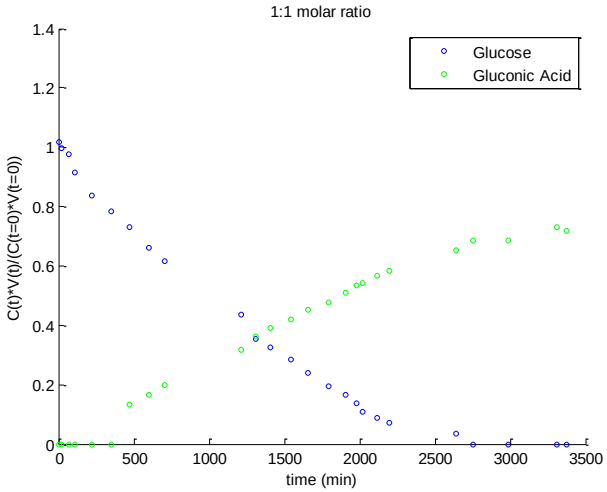

Figure 17: Mass balance checking for glucose in a 1:1 molar ratio experiment.

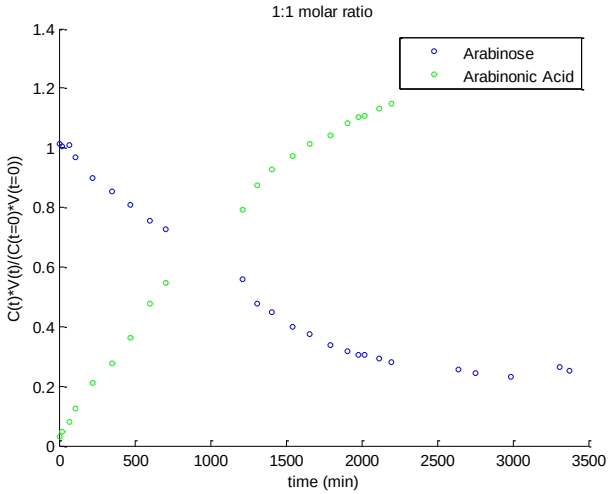

Figure 18: Mass balance checking for Arabinose in a 1:1 molar ratio experiment.

- 1 Arabinose: 2 Glucose molar ratio

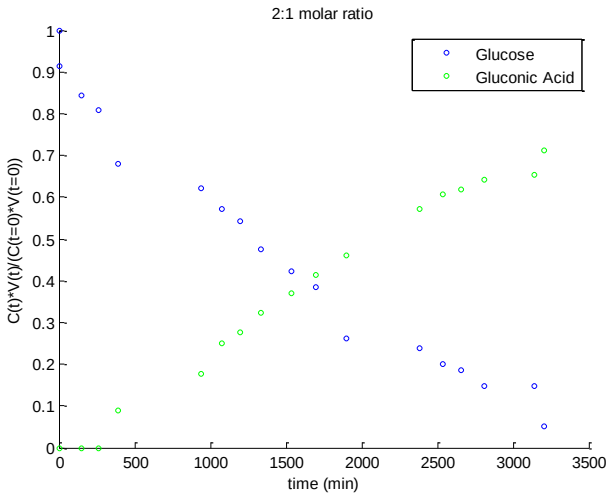

Figure 19: Mass balance checking for glucose in a 2:1 molar ratio experiment.

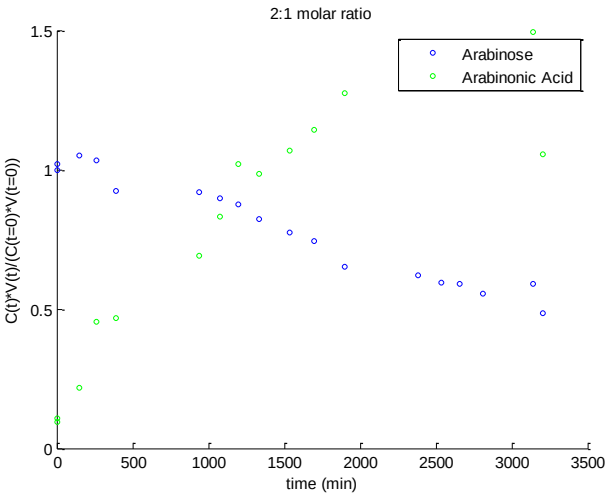

Figure 20: Mass balance checking for Arabinose in a 2:1 molar ratio experiment.

- 2 Arabinose: 1 Glucose molar ratio

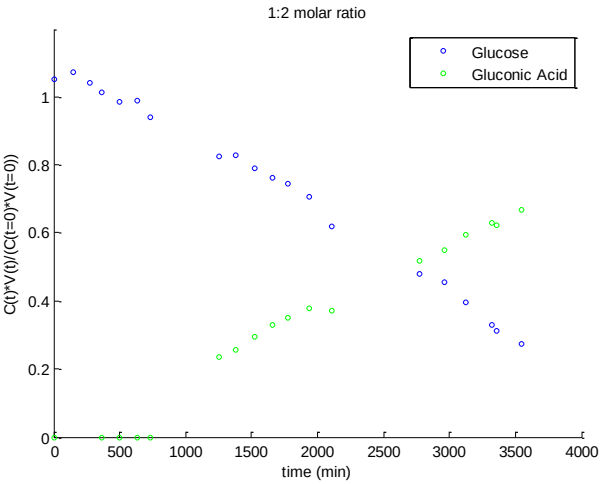

Figure 21: Mass balance checking for glucose in a 1:2 molar ratio experiment.

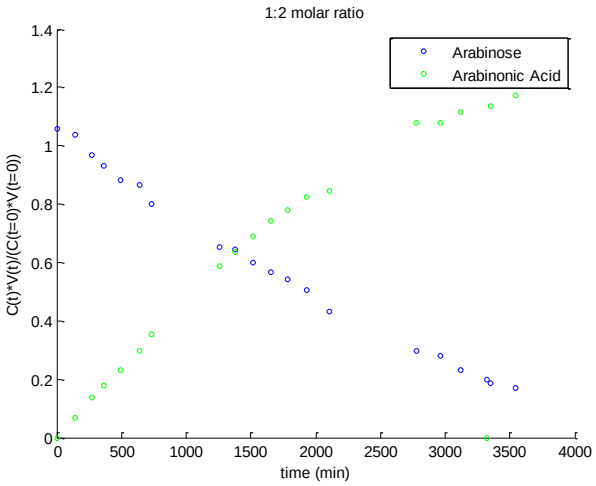

Figure 22: Mass balance checking for Arabinose in a 1:2 molar ratio experiment.

From the mass balance it can be concluded that the selectivity of glucose to gluconic acid is not 100%, but some of the glucose is oxidazed to glucoronic acid and other minoritary by-products. Note that the isomerization compound of arabinose, ribulose, it is also included in the peak of the gluconic acid. Furthermore, arabinose and arabinonic acid do not follow the total mass balance, which indicates that there is a by-product originating from glucose which has a residence time similar to that of arabinonic acid in the HPLC analisys. The experiments show the same pattern. However, the second experiment, 2:1 glucose-to-arabinose presents some errors, which can be originated in the experimental process.

5.1.3. Carbon catalyst

In the previous work of this project [26], the sugar oxidation was performed by a different kinds of catalysts. Some of them were supported by alumina and other ones on N-mesoporous carbon. In the N-C- mesoporous catalyst, the cluster size of the gold nanoparticles was 10 times larger, 20-30 nm meanwhile gold nanoparticles on alumina were between 2-3 nm. The reaction was conducted normally with the small cluster size. The catalyst was inactive showing low reaction rates. Knowing that the optimal cluster size for the gold nanoparticles to be active in oxidation reactions is around 2 nm, it might be suggested that the support of the catalyst can be active for the oxidation. This suggestion is a step forward for the project due to the low price of carbon compared to gold. Therefore, an experiment was carried out using the N-C-mesoporous material without any gold content.

The reaction was performed under standard conditions, 70ºC, ph 8, 0.125 atm oxygen partial pressure, stirring speed exceeding 900 rpm, and 0.1 g of N-C-mesoporous catalyst crushed using a porcelain mortar and pestle prior to the experiment.

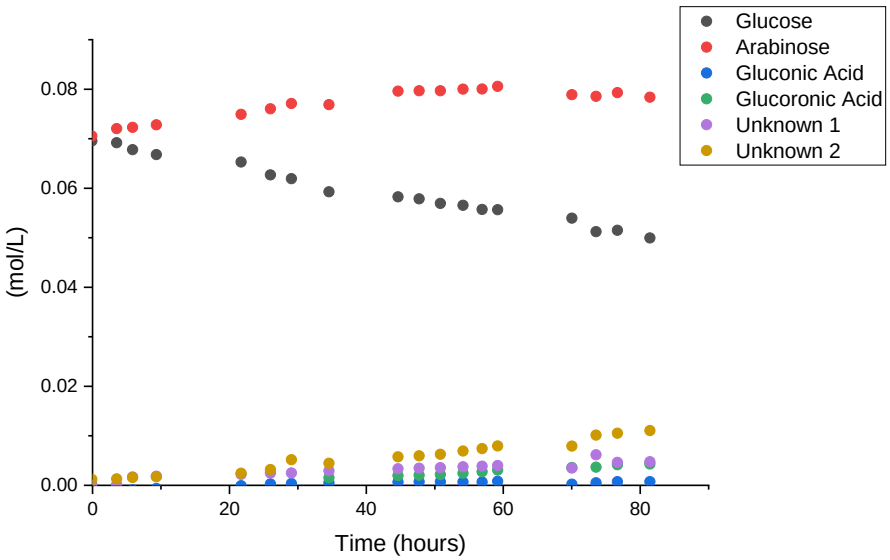

Figure 23: Oxidation reaction with N-C mesoporous catalyst.

The experiment was continued 80 hours observing a slight activity in the oxidation. The results are displayed in Figure 23. The increase of the arabinose concentration is due to the isomerization of glucose to fructose. However, the glucose consumption is higher than the concentration increase of the arabinose, so evidently, some part of the glucose is reacting to gluconic acid and glucuronic acids. The presence of different products in the reaction was confirmed by HPLC. To summarise the experimental experience, this catalyst shows a low activity for sugar oxidation but however, it is an inexpensive catalyst. It would be very interesting to investigate more deeply how it is working and what the selectivities and conversions are in the space of experimental parameters.

5.2. Catalyst characterization

5.2.1. TEM

The metal particles were characterized with transmission electron microscopy (TEM) (JEOL JEM-1400Plus) equipment. This analysis provides nanoscale images of particles with a high resolution. A lot of information can be acquired from this technique, for instance, average particle size, particle size distribution, nanoparticle dispersion and morphology. Two different samples were analysed using this method. The fresh and the expend catalyst collected after

the reaction were studied, both of them were of the extrudate shape. The particle size distributions were calculated with the software ImageJ. The results are shown in Figures 24 and 25.

- Fresh Catalyst

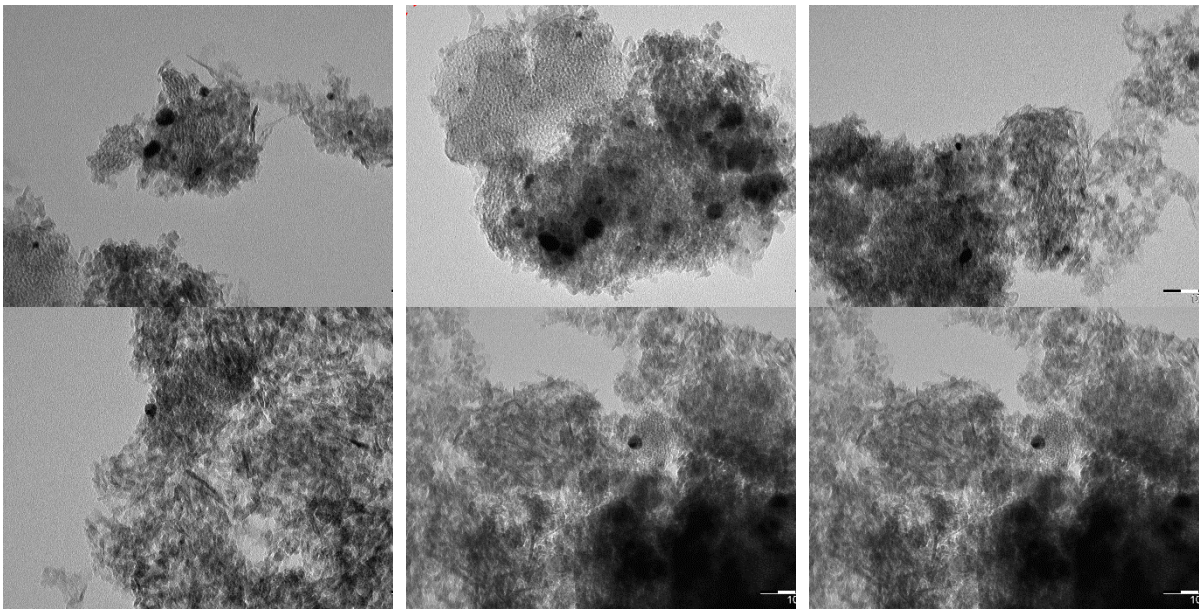

Figure 24: TEM image for fresh catalyst sample.

The fresh catalyst was impossible to analyse due to the poor quality of the images obtained from the TEM analysis, because too small amounts of particles were at disposal for the measurement. However, the general conclusion is that the sizes of the nanoparticles were 2-3 nm.

- Spent Catalyst

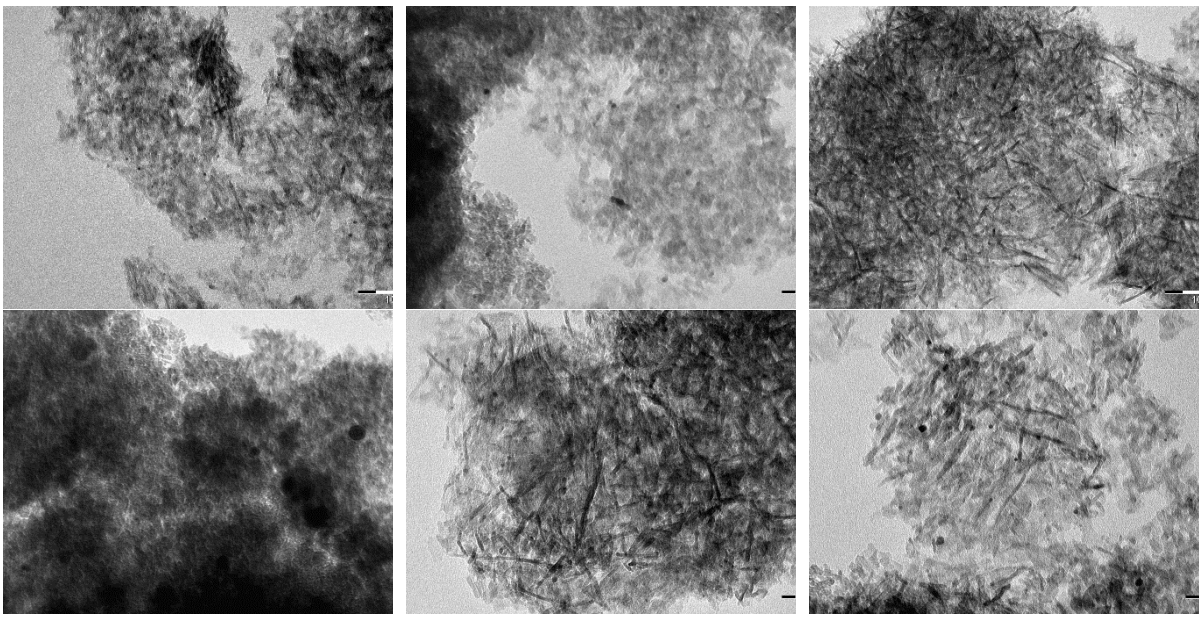

Figure 25: TEM images for a spent catalyst sample.

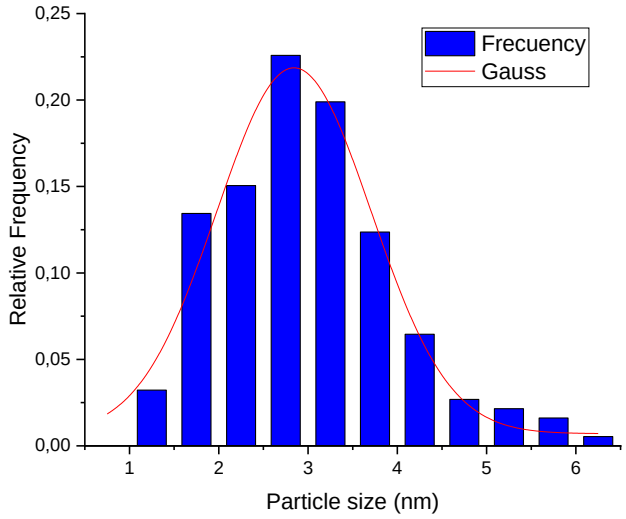

Figure 26: Particle size distribution at a spent catalyst.

The particle size distribution of the spent catalyst was determined by TEM to reveal whether there is any change after the reaction, such as particle agglomeration, which can appear after the oxidation process. The distribution diagram is presented in Figure 26. From the particle size analysis, it was confirmed that the average size was 3 nm, which is in accordance with the specifications of the fresh catalyst.

6. MODELING OF SIMULTANEOUS KINETIC AND DIFFUSION EFFECTS

The use of the Spinchem device should suppress external mass transfer limitations because of very intensive stirring and turbulence around the catalyst particles, so the issue is the quantitative interpretation of the experimental data to understand how the internal mass transfer limitation, i.e. diffusion inside the catalyst pores affects the overall kinetics. Moreover, it is important to check whether the amount of oxygen supplied is enough to saturate the liquid phase.

The oxygen solubility is strongly dependent on the temperature and the amount of the dissolved electrolyte. In both cases, they are inversely proportional magnitudes, which means increasing the temperature or the concentration of the electrolyte, the solubility will decrease. The expression below gives the concentration of dissolved oxygen as a function of pressure and temperature in pure water [30,31]. Considering partial pressure of oxygen (0.125 atm) and temperature (343.15 K), we obtain

$$C_{O2} = \frac{55.56\ P_{O2}}{\exp\left(3.71814 + \frac{5596.17}{T} - \frac{1049668}{T^2}\right) - P_{O2}} = 1.03 * 10^{-4} mol/dm^3 \qquad \textit{Ec. 1}$$

Something to be kept in the mind is that the system is not pure water, it is at pH 8 and has dissolved sodium and hydroxide ions. The dissolved electrolyte salt usually decreases the solubility of oxygen, and henry's constant for the pure solvent can be corrected using the salting-out factor of the electrolyte dissolved using the following equation:

$$\ln \frac{H}{H_0} = \sum (h_i + h_G)\, c_i$$

The oxygen flow in the experiments was 5 mL/min and inside the reactor, the system remained under constant conditions at 70ºC and 1 atm and the maximum liquid volume never exceeded 250 mL, which was the most restrictive situation. Under these conditions, the oxygen flow was fed at $1.77*10^{-4}$ mol/min and assuming the maximun volume of 250 ml which is not reached in any case the flux would be $7.11*10^{-4}$ mol/(L·min)

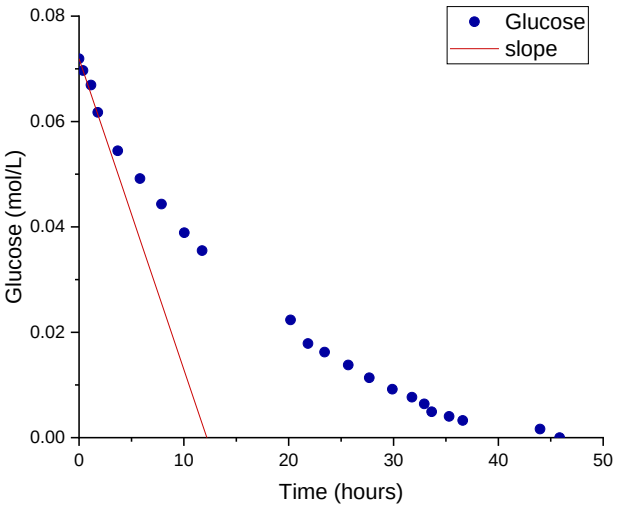

Figure 27: Oxygen requirements for glucose.

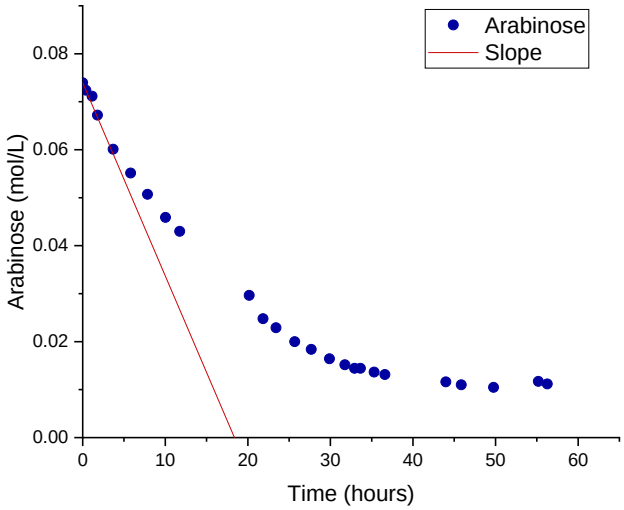

Figure 28: Oxygen requirements for arabinose.

The slopes displayed in Figures 27-28 show the amount of oxygen needed per volume and time for each component. The addition of the slopes represents the total oxygen flow requirement. The total slope has a value of $1.65*10^{-4}$ mol/(L·min).

Comparing the experimental data of the oxygen feed, 7.11*10-4 mol/(L·min) to the initial rate 1.65*10-4 mol/(L·min), it can be concluded that the oxygen feed flow guarantees the saturation of oxygen in the liquid phase.

6.1. Kinetic model

A simplified kinetic model is needed where just the main reactions are considered. The model is based on the following stoichiometry,

$$Gluc + {}^{1}/_{2}\, O_2 \rightarrow GlucO \qquad \textit{R. 1}$$

$$Ara + {}^{1}/_{2}\, O_2 \rightarrow AraO \qquad \textit{R. 2}$$

$$Gluc + {}^{1}/_{2}\, O_2 \rightarrow GlucRO \qquad \textit{R. 3}$$

$$Gluc \rightarrow Fruc \qquad \textit{R. 4}$$

$$Ara \rightarrow Rib \qquad \textit{R. 5}$$

Moreover, in the derivation of the rate equations, the adsorption of the compounds on the catalyst surface are taken into account. The following reactions describe the adsorption of the reactants,

$$Gluc + * \leftrightarrow Gluc* \qquad \textit{R. 6}$$

$$Ara + * \leftrightarrow Ara* \qquad \textit{R. 7}$$

$$O_2 + * \leftrightarrow O_2* \qquad \textit{R. 8}$$

In this model the main reaction from the sugar to the corresponding sugar acid (R.1 and R.2) is considered. Also the formation of the by-product from the glucose, glucuronic acid (R.3) for which a very low kinetic constant was observed, is included in the model, i.e. the isomerization of glucose and arabinose to fructose and ribulose (R.5 and R.6). Molecular adsorption of oxygen is presumed and the adsorption steps are assumed to be in quasi-equilibria, while the surface reaction steps are considered to be rate limiting. Based on these hypotheses, the mass balances of the components are summarized below,

$$\frac{dN_{\text{gluc}}}{dt} = r_{\text{gluc}} = -(R_1 + R_3 + R_4)\, m_{cat} \qquad \textit{Ec. 4}$$

$$\frac{dN_{\text{Ara}}}{dt} = r_{\text{Ara}} = -(R_2 + R_5)\, m_{cat} \qquad \textit{Ec. 5}$$

$$\frac{dN_{\mathrm{glucO}}}{dt} = r_{\mathrm{glucO}} = R_1\ m_{cat} \quad \textit{Ec. 6}$$

$$\frac{dN_{\mathrm{AraO}}}{dt} = r_{\mathrm{AraO}} = R_2\ m_{cat} \quad \textit{Ec. 7}$$

$$\frac{dN_{\mathrm{glucRO}}}{dt} = r_{\mathrm{GlucRO}} = R_3\ m_{cat} \quad \textit{Ec. 8}$$

$$\frac{dN_{\mathrm{fruc}}}{dt} = r_{\mathrm{fruc}} = R_4\ m_{cat} \quad \textit{Ec. 9}$$

$$\frac{dN_{\mathrm{rib}}}{dt} = r_{\mathrm{rib}} = R_5\ m_{cat} \quad \textit{Ec. 10}$$

$$r_{\mathrm{O2}} = -(R_1 + R_2 + R_3)\ m_{cat} \quad \textit{Ec. 11}$$

The surface reaction kinetics is given by the expressions

$$R_1 = k_1\theta_{\mathrm{Gluc}}\theta_{\mathrm{O2}} \quad \textit{Ec. 12}$$

$$R_2 = k_2\theta_{\mathrm{Ara}}\theta_{\mathrm{O2}} \quad \textit{Ec. 13}$$

$$R_3 = k_3\theta_{\mathrm{Gluc}}\theta_{\mathrm{O2}} \quad \textit{Ec. 14}$$

$$R_4 = k_4\theta_{\mathrm{Gluc}} \quad \textit{Ec. 15}$$

$$R_5 = k_5\theta_{\mathrm{Ara}} \quad \textit{Ec. 16}$$

In the mathematical modelling, the ordinary differential equations (4) - (10) were solved using the amounts of substance (molar amounts) instead of concentrations due to the volume change during the reaction. The main reason for the volume change is the addition of NaOH into the reaction mixture for the pH adjustment.

The total mass balance of the active sites on the catalyst should be one while the coverage of each compound on the catalyst surface is proportional to the concentration of the compound inside the pores, according to the ideal adsorption theory of Langmuir,

$$\theta_{\mathrm{i}} = k_{\mathrm{i}}\mathrm{C_i}\theta_{\mathrm{v}} \quad \textit{Ec. 17}$$

$$\sum \theta_{\mathrm{i}} = 1 \quad \textit{Ec. 18}$$

From this ideal adsorption theory and the presumption of rate limiting steps, the rate equations can be expressed as

$$R_1 = \frac{k_1\mathrm{C_{Gluc}}C_{\mathrm{O2}}}{(1 + K_{\mathrm{Glu}}C_{\mathrm{Gluc}} + K_{\mathrm{Ara}}\mathrm{C_{Ara}} + K_{\mathrm{O}}\mathrm{C_{O2}})^2} \quad \textit{Ec. 19}$$

$$R_2 = \frac{k_2 C_{\mathrm{Ara}} C_{\mathrm{O2}}}{(1 + K_{\mathrm{Glu}} C_{\mathrm{Gluc}} + K_{\mathrm{Ara}} C_{\mathrm{Ara}} + K_{\mathrm{O}} C_{\mathrm{O2}})^2} \qquad \textit{Ec. 20}$$

$$R_3 = \frac{k_3 C_{\mathrm{Gluc}} C_{\mathrm{O2}}}{(1 + K_{\mathrm{Glu}} C_{\mathrm{Gluc}} + K_{\mathrm{Ara}} C_{\mathrm{Ara}} + K_{\mathrm{O}} C_{\mathrm{O2}})^2} \qquad \textit{Ec. 21}$$

$$R_4 = \frac{k_4 C_{\mathrm{Gluc}}}{1 + K_{\mathrm{Glu}} C_{\mathrm{Gluc}} + K_{\mathrm{Ara}} C_{\mathrm{Ara}} + K_{\mathrm{O}} C_{\mathrm{O2}}} \qquad \textit{Ec. 22}$$

$$R_5 = \frac{k_5 C_{\mathrm{Ara}}}{1 + K_{\mathrm{Glu}} C_{\mathrm{Gluc}} + K_{\mathrm{Ara}} C_{\mathrm{Ara}} + K_{\mathrm{O}} C_{\mathrm{O2}}} \qquad \textit{Ec. 23}$$

A preliminary approach to the experimentally observed kinetics is to prepare a first order test plot of the experimental data. The results of this preliminary analysis are displayed in Figures 29-30. The test plot is based on the normalized logarithmic concentrations versus the reaction time. If the plot is linear, the system follows first-order kinetics with respect to the sugar concentration.

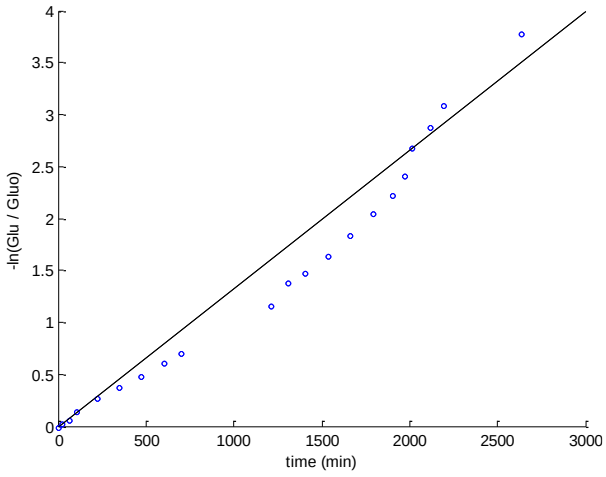

Figure 29: First order kinetic comparison glucose.

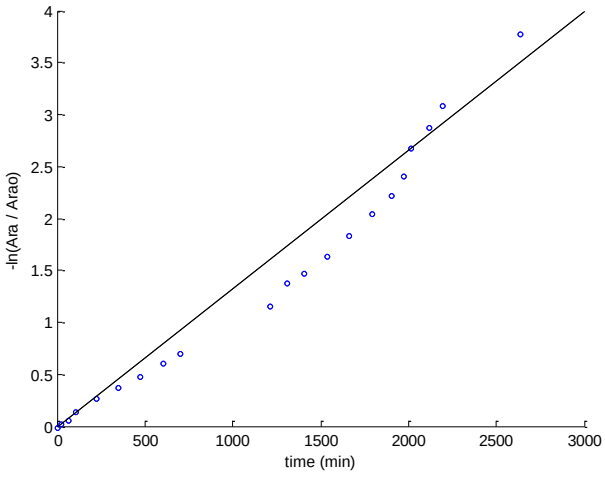

Figure 30: First order kinetics comparison arabinose.

The clear deviation upwards from the logarithmic plots confirms that the effective reaction order with respect of the sugar concentration is less than one. This is in agreement with the mechanistic rate equations (19) - (23) and from the chemical viewpoint, because this deviation from first order kinetics can be explained by adsorption of the sugar molecules on the catalyst surface. As the reaction progresses, the sugar concentration decreases and the effective reaction order approaches one [32].

To test the reliability of the kinetic model proposed, it was solved numerically with Matlab. The estimation of the apparent kinetic constants without taking into account the mass transfer limitations inside the catalyst pores will give an idea about the accuracy of the preliminary approach. The optimization problem was solved by the minimization of the objective function

$$Q = \sum_{i=1}^{n}\sum_{j=1}^{m}(C_{\exp i,j} - C_{\mathrm{est}\,i,j})^2 \qquad \textit{Ec. 24}$$

Keeping in mind that the volume was continuously increasing due to the adding of sodium hydroxide during the experiment, three different approaches were applied for just one experiment in order to compare the best fit: constant liquid volume, linear dependence on time and interpolation of the real data of the NaOH addition.

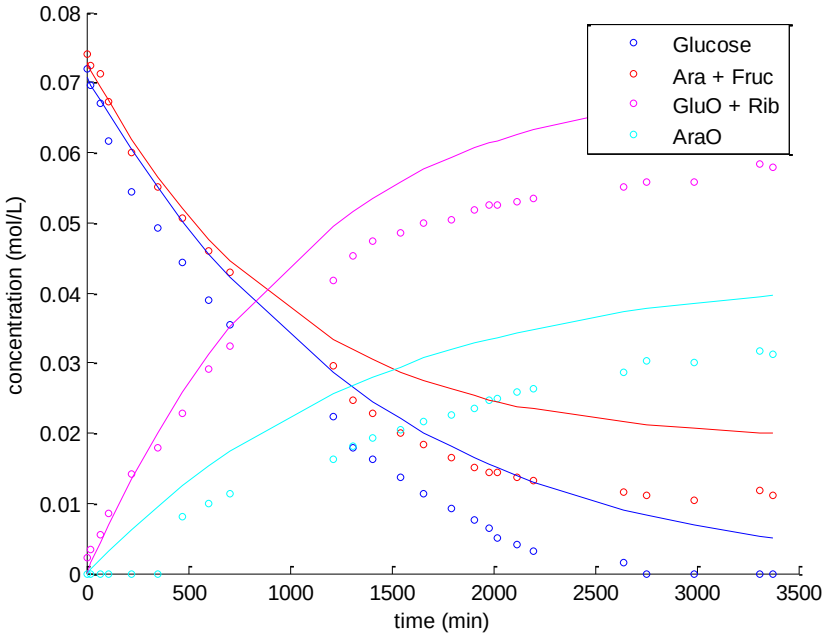

Figure 31: Kinetic model of experiment 1:1 molar ratio using constant volume approximation.

The modelling approach using a constant liquid volume (initial volume 0.150L) had a higher deviation due to the increasing of the volume during the reaction time, which decreases the concentrations of the reactants and products. This effect was not taken into account in the kinetic modelling so the curves stay above the experimental data, with an increasing discrepancy with time.

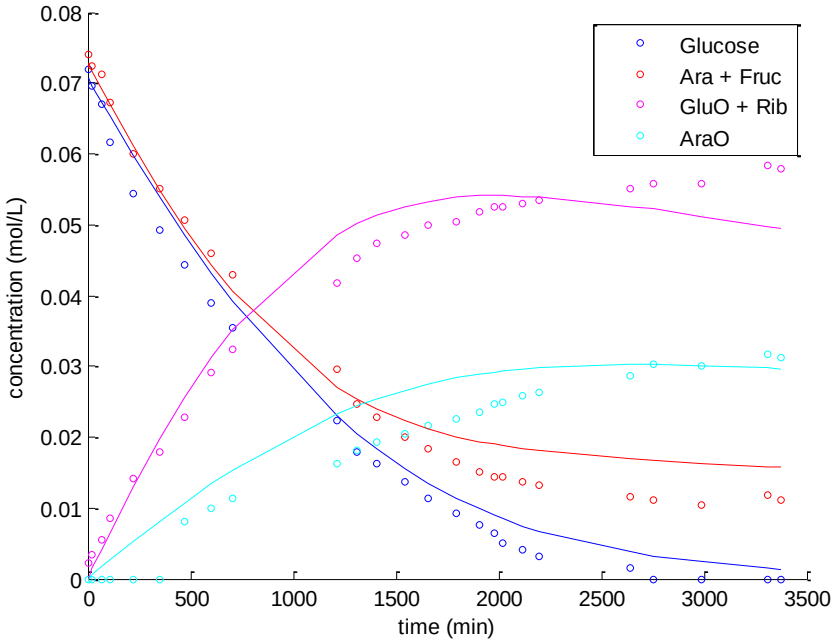

Figure 32: Kinetic model of experiment 1:1 molar ratio using linear dependence volume approximation.

Using the linear approximation of the volume over time, the fit improved to some extent. However, as the evolution of the volume over time is not even similar to a straight line, the kinetic curve takes a shape that does not correspond to the experimental data. The dependence between volume and time presents a clear exponential trend, which can be solved analytically obtaining an exponential relationship

For first order model

$$V\,(t) = V_{\infty}(1 - e)^{-\tau/t} \qquad \textit{Ec. 25}$$

or for this system specifically

$$V\,(t) = \left(\frac{C_{\mathrm{oGlu}} - C_{\mathrm{Glu}}(t) + C_{\mathrm{oAra}} - C_{\mathrm{Ara}}(t)}{C_{\mathrm{oGlu}} - C_{\mathrm{Glu}\infty} + C_{\mathrm{oAra}} - C_{\mathrm{Ara}\infty}}\right) V_{\infty} \qquad \textit{Ec. 26}$$

It should be kept in mind that the equations presented above are approximations, but not exact ones.

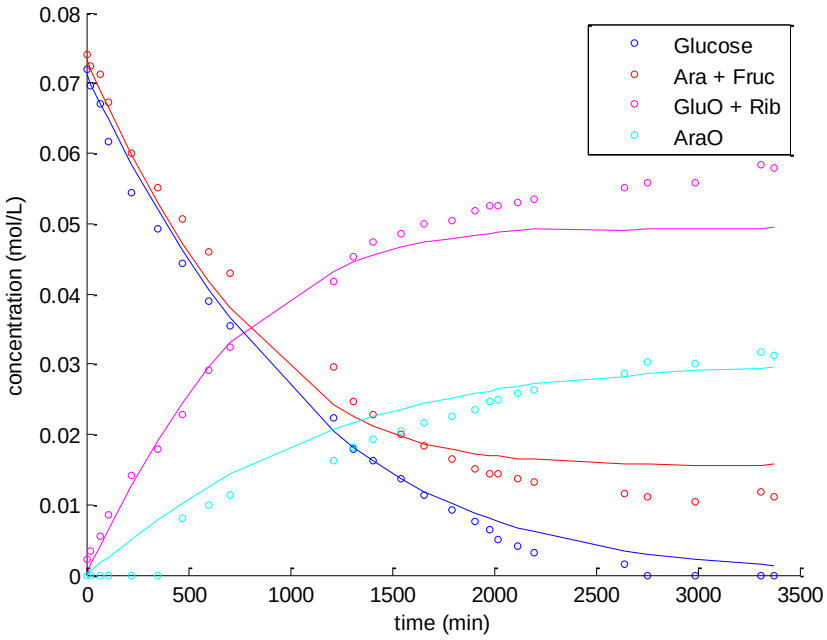

Figure 33:Kinetic model of experiment 1:1 molar ratio using real data volume.

An interpolation from the real volume data from the experiment gives the best accuracy for the modelling as can be seen from Figure 33. There is still some deviation at the end of the experiment, which can be explained by the formation of oligomers, which are not taken into account in this modelling effort.

The kinetic constants obtained for the experiment using this approximation of the volume are the following ones:

K_1	278.1802 $m^3/(g_{Au}\ s)$	K_5	0.0001 $m^3/(g_{Au}\ s)$
K_2	693.8352 $m^3/(g_{Au}\ s)$	K_O	178.1196 $m^3/(g_{Au}\ s)$
K_3	15.0206 $m^3/(g_{Au}\ s)$	K_{Glu}	108.0938 $m^3/(g_{Au}\ s)$
K_4	0.6671 $m^3/(g_{Au}\ s)$	K_{Ara}	851.0752 $m^3/(g_{Au}\ s)$

For the complete kinetic model, a selected set of experiments will be used.

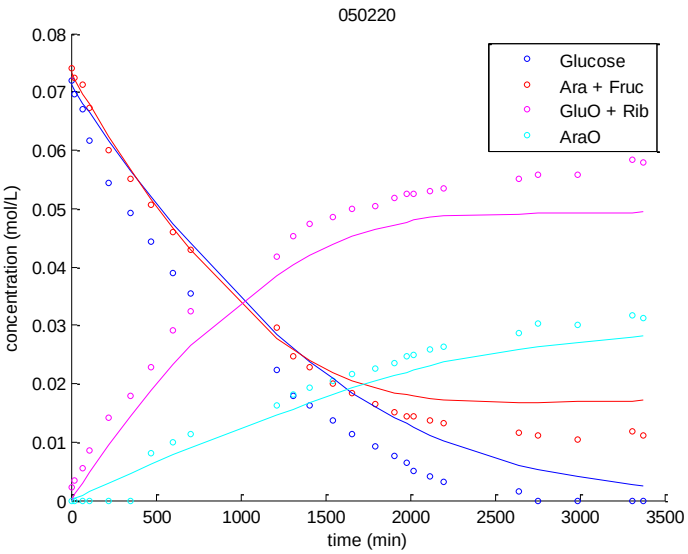

Figure 34: Fitting of 1:1 molar ratio oxidation of glucose and arabinose over nano gold particles at 70°C

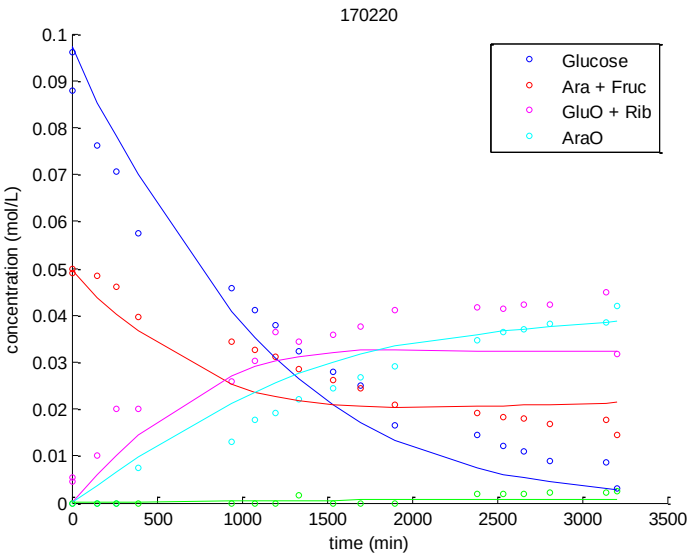

Figure 35:Fitting of 2:1 molar ratio oxidation of glucose and arabinose over nano gold particles at 70°C

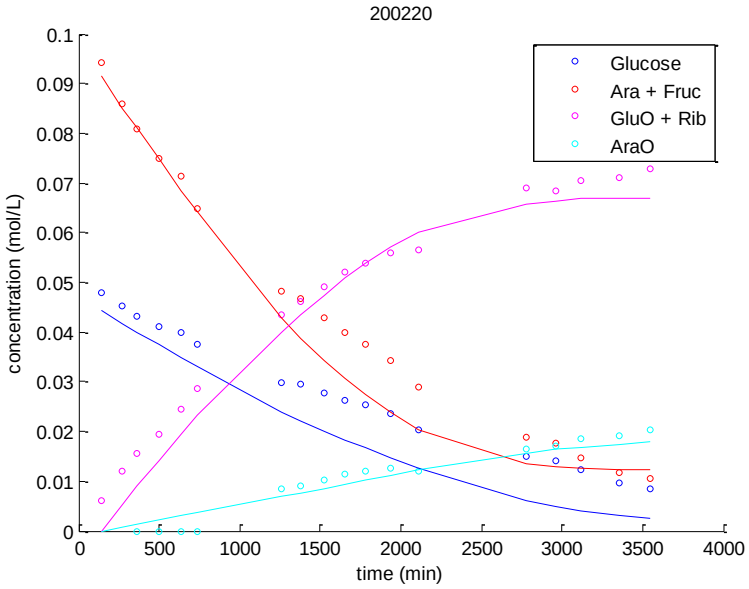

Figure 36: Fitting of 1:2 molar ratio oxidation of glucose and arabinose over nano gold particles at 70°C

Giving the following rate constants and performing the reaction as it is shown in the plot:

K_1	224.1257 $m^3/(g_{Au}\ s)$	K_5	7.3496 $m^3/(g_{Au}\ s)$
K_2	717.6418 $m^3/(g_{Au}\ s)$	K_O	162.5694 $m^3/(g_{Au}\ s)$
K_3	4.1670 $m^3/(g_{Au}\ s)$	K_{Glu}	29.3569 $m^3/(g_{Au}\ s)$
K_4	0.6075 $m^3/(g_{Au}\ s)$	K_{Ara}	1610.1107 $m^3/(g_{Au}\ s)$

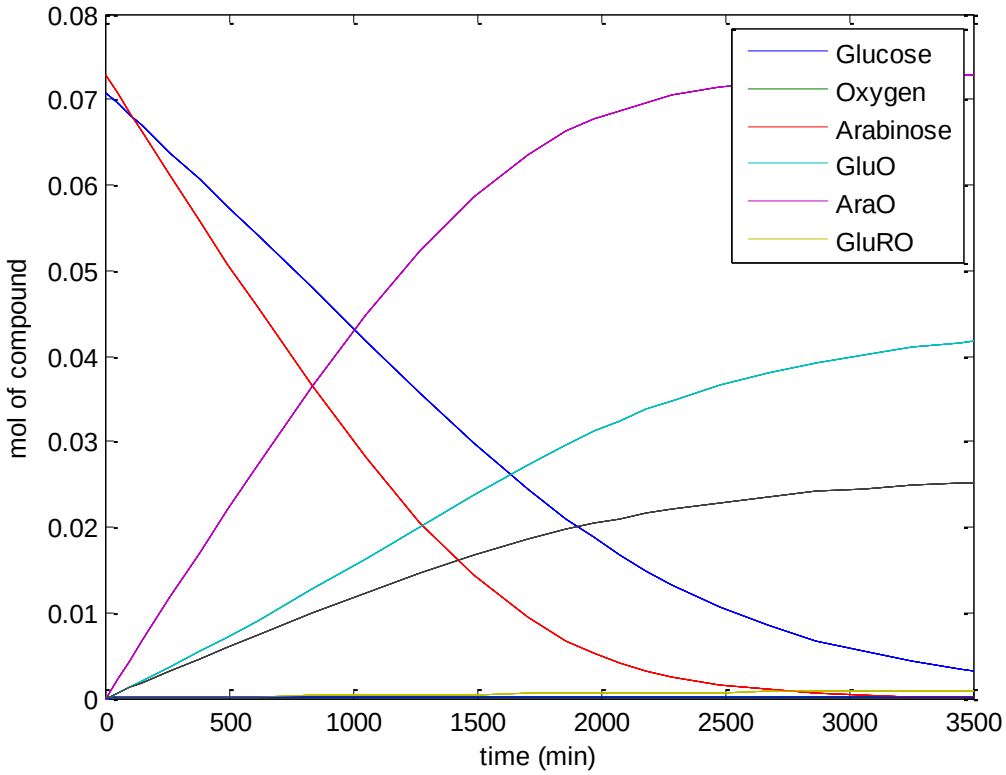

Figure 37: Predicted behaviour of the oxidation of arabinose and glucose to the correspondent sugar acids at 70ºC.

The mathematical model describes the general behaviour of the oxidation of arabinose and glucose mixture on the gold catalyst extrudates. The model could be refined, improving the current method of analysis, by measuring the concentrations of each component. Giving a more accurate information of the amount of oligomers present in the solution and avoiding the overlapping of substances during their analysis might be the next step.

6.2. Diffusion and reaction in porous catalyst particles

The mass balance for a component (i) inside a porous catalyst with radius (r) depends on the diffusion flux (N_i) and the reaction rate (r_i) of each component. It can be written as [33]

$$\varepsilon_p \frac{dC_i}{dt} = -\frac{d(N_i r^s)}{r^s dr} + r_i \rho_p \qquad \textit{Ec. 27}$$

The general shape factor (s) is a dimensionless number which defines the ratio between the reaction rate and the intensity of the mass transport inside the particle [34]. It is a function of the outer surface area and the volume of the particle;

$$s + 1 = \left(\frac{A_P}{V_P}\right) R \qquad \textit{Ec. 28}$$

For a cylindrical catalyst particle with the radius (R) and the length (L) the surface area is A_P = 2 πR^2+ 2 πRL and the volume is $V_P = \pi R^2 L$.

$$s = 2\left(\frac{R}{L}\right) + 1 \qquad \textit{Ec. 29}$$

For a long cylinder in which the length is much higher than the radius, the ratio R/L is tiny, thus s can be approached to 1.

The extended description of the diffusion is based on the molecular diffusion and Knudsen diffusion theories. The Maxwell- Stefan approach provides a general set of equations for describing mass transfer [35].The detailed concept can be found in many textbooks of chemical engineering e.g. [36–38]. Knudsen diffusion prevails when the gas density is low and the pores are small, but Knudsen diffusion is not observed in liquids solutions [33]. From the studies presented by Salmi and Wärnå [39] where is showed the comparison of different diffusion methods, it can be concluded that a simplified method using the individual effective diffusion coefficients as a function of the local concentration of each component inside the pore is very accurate.

The simplest description of the diffusion is Fick's law, where the flux is assumed to be proportional to the concentration gradient,

$$N_{\mathrm{i}} = -D_{\mathrm{ei}}\frac{dC_{\mathrm{i}}}{dr} \qquad \textit{Ec. 30}$$

Replacing in the equation Ec.27 gives

$$\varepsilon_{\mathrm{p}}\frac{dC_{\mathrm{i}}}{dt} = \frac{d\left(D_{\mathrm{e}i}\frac{dC_{\mathrm{i}}}{dr}r^{s}\right)}{r^{s}dr} + r_{\mathrm{i}}\rho_{\mathrm{p}} \qquad \textit{Ec. 31}$$

Assuming that the effective diffusion coefficient (D_{ei}) is constant for each local concentration, the equation obtains a differentiated form

$$\varepsilon_{\mathrm{p}}\frac{dC_{\mathrm{i}}}{dt} = D_{\mathrm{ei}}\left(\frac{d^2C_{\mathrm{i}}}{dr^2} + \frac{s}{r}\frac{dC_{\mathrm{i}}}{dr}\right) + r_{\mathrm{i}}\rho_{\mathrm{p}} \qquad \textit{Ec. 32}$$

A dimensionless coordinate is introduced instead of the particle radius giving the following equation

$$\varepsilon_{\mathrm{p}}\frac{dC_{\mathrm{i}}}{dt} = \frac{D_{\mathrm{ei}}}{R^2}\left(\frac{d^2C_{\mathrm{i}}}{dx^2} + \frac{s}{x}\frac{dC_{\mathrm{i}}}{dx}\right) + r_{\mathrm{i}}\rho_{\mathrm{p}} \qquad \textit{Ec. 33}$$

The boundary conditions as well as initial conditions allow the equations to be solved by robust numerical methods.

At the initial state, the concentration inside the particle of each component is presumed to be zero.

The concentration gradients at the centre of the particle are zero at any time during the reaction because of symmetry reasons and the concentrations at the outer surfaces of the

particles are equal to the concentrations in the bulk phase because of high stirring speed. The boundary conditions are summarized in the following equations

$$C_{\mathrm{i}}(t=0)=0, \qquad x\,\epsilon\,[0,1] \qquad \textit{Ec. 34 (a-b)}$$
$$C'_{\mathrm{i}}(t=0)=0, \qquad x\,\epsilon\,[0,1]$$

$$C_{\mathrm{i}}(t)=C'_{\mathrm{i}}(t)\,, \qquad x=1 \qquad \textit{Ec. 35 (a-b)}$$
$$\frac{dC_{\mathrm{i}}}{dx}=0, \qquad x=0$$

The model equations along with initial and boundary conditions are solved by the numerical method using the method of lines, which implies the discretization of the space derivatives with finites differences. Consequently, a large system of ordinary differential equations (ODEs) are created and they can be solved with robust algorithms for stiff ordinary differential equations (ODEs), as initial value problems (IVPs)

However, introducing the quasi-steady state approach, equation 33 It can be integrated numerically as follows,

$$\frac{dC_{\mathrm{i}}}{dt}=0 \qquad q.e \qquad \textit{Ec. 36}$$

$$-\int_0^{y} d\left(D_{\mathrm{e}i}\frac{dC_{\mathrm{i}}}{dr}r^{s}\right)=\int_0^{R} r_{\mathrm{i}}\rho_{\mathrm{p}}r^{s}dr \qquad \textit{Ec. 37}$$

where y corresponds to the value of Dei dCi/dr rs at r=R at the external surface area of the catalyst. Turning to the dimensionless coordinate the integral can be written as

$$-d\left(D_{\mathrm{e}i}\frac{dC_{\mathrm{i}}}{dr}r^{s}\right)=\int_0^{1} r_{\mathrm{i}}\rho_{\mathrm{p}}(Rx)^{s}Rdx \qquad \textit{Ec. 38}$$

The particle density and radius are constant; thus they can be extracted from the integral, leaving us with the expression:

$$-D_{\mathrm{e}i}\frac{dC_{\mathrm{i}}}{Rdx}=R\rho_{\mathrm{P}}\int_0^{1} r_{\mathrm{i}}x^{s}dx \qquad \textit{Ec. 39}$$

The term $D_{\mathrm{e}i}$ dC_i/Rdx corresponds to the diffusion flux inside the catalyst particle (N_i), which becomes

$$N_{\mathrm{i}} = R\rho_{\mathrm{P}} \int_0^1 r_{\mathrm{i}} x^{\mathrm{s}} dx \qquad \textit{Ec. 40}$$

In case the system is governed exclusively by the intrinsic kinetics, there were no significant diffusion limitations throughout the particle, the rate expression could be removed outside from the integral and the expression for intrinsic kinetic control becomes

$$N_{\mathrm{i}} = \frac{R\rho_{\mathrm{P}} r_{\mathrm{i}}}{s+1} \qquad \textit{Ec. 41}$$

Because of the results obtained from the experiments with different particle sizes, the absence of internal diffusion limitations cannot be assumed, but the numerical solution of equation 33 is required.

6.3. Diffusion coefficients in the liquid phase

The diffusion inside a porous particle is proportional to the concentration gradient. This proportionality coefficient is called the diffusion coefficient and it is specific for each compound.

To estimate the diffusion coefficient for the components it will be assumed that molecular diffusion is due to the liquid-phase system. The Wilke-Chang equation [40–43] is used among the numerous models for the liquid-phase diffusion coefficients. The experiments were conducted with a porous catalyst, and consequently, the particle tortuosity and porosity will be used to get the numerical value of the effective diffusion coefficient.

We consider the solution as pure water, because the concentration of sugars or sodium hydroxide is very low. The Wilke-Chang equation gives

$$D = \frac{7.4 * 10^{-8} (X * M)^{1/2}\, T}{\mu\, \tilde{V}^{0.6}} \qquad \textit{Ec. 42}$$

$$D_{\mathrm{ei}} = \frac{\varepsilon}{\tau} D \qquad \textit{Ec. 43}$$

where the association parameter for water is 2.6, the temperature of the reaction is 343.15 K, the viscosity of the solution is 0.350 cP [37]. The pore radius and the porosity are given by the nitrogen physisorption analysis which are 55 Å and 0.39 respectively.

The tortuosity factor is used to correct the diffusion coefficient for the non-linear structures of the pores; this property gives us an idea about real paths through which the molecules diffuse. This value is difficult to approach bus some studies reports values from 2 to 3 for the alumina support [44,45]. Thus the tortuosity factor of 2.5 was assumed in further calculations.

6.4. Mass transfer in the liquid bulk phase

Each chemical compound, reactant and product, is diluted in the aqueous phase, and the concentrations of these products depend on the reaction time. Except for the oxygen which was continuously fed to the system ensuring the saturation in the liquid phase. Thus, the oxygen concentration remained constant and can be neglected from the mass balances. The high stirring speed removed completely the external mass transfer limitations. Based on these facts, the mass balance for the sugars and the oxidation products can be written as

$$\frac{dn'_{\mathrm{i}}}{dt} = N_{\mathrm{i}} A'_{\mathrm{P}} \qquad \textit{Ec. 44}$$

where A'_P represents the total outer surface of the catalyst particle, N_i is the flux at the outer surface of the particle and n_i denotes the amount of substance (in moles) of each compound. For the particle area and diffusion flux is valid for catalyst particles of equal sizes,

$$A'_{\mathrm{P}} = n_{\mathrm{P}} A_{\mathrm{P}} \qquad \textit{Ec. 45}$$

$$N_{\mathrm{i}} = -\frac{D_{\mathrm{ei}}}{R}\left(\frac{dC_{\mathrm{i}}}{dx}\right)_{x=1} \qquad \textit{Ec. 46}$$

The amount of each compound depends on the concentration and the liquid volume as a function of the reaction time,

$$\frac{dn'_{\mathrm{i}}}{dt} = V_{\mathrm{L}}\frac{dc'_{\mathrm{i}}}{dt} + c'_{\mathrm{i}}\frac{dV_{\mathrm{L}}}{dt} = N_{\mathrm{i}} A'_{\mathrm{P}}$$

The liquid volume can be calculated by interpolation of the real experimental data, taking into account the decrease of the liquid volume due to the sampling. So as a discrete variable, the volume can be calculated as

$$V_{\mathrm{L}}(t) = V_{\mathrm{Lo}} + \int_0^t V_{\mathrm{add}} dt - V_{\mathrm{sampling}}(t)$$

7. CONCLUSION AND FUTURE PERSPECTIVES

Besides all the problems from the overlapping peaks of components in the HPLC analysis, the results of the sugar oxidation experiments, the results might lead fundamental conclusions on the oxidation of arabinose and glucose on supported gold catalyst. Knowing that this heterogeneously catalysed oxidation is a viable process to valorize lignocellulosic biomass for obtaining sugar acids. Gold represents a workable catalyst material, both in the form of powder and extrudates. The experiments conducted in this project elucidated the potential of the gold catalyst but also the disadvantages, the catalyst deactivation. The main reason for catalyst deactivation might be leaching of the active metal to the liquid phase

One of the main goals was to study the interaction of intrinsic oxidation kinetics and the internal mass transfer in the oxidation process. The experimental results showed a very strong retarding effect of the internal mass transfer resistance inside the catalyst pores. Kinetic and mass transfer models were considered in the present work to analyse the interaction of intrinsic kinetics and internal mass transfer.

Some additional research work is still needed to complete this very demanding interdisciplinary research project. To obtain more reliable data, the overlapping problem in the HPLC analysis should be fixed to study more deeply the isomerization of glucose and arabinose. The compounds, which participate in these reactions have similarities in the structures that impairs the separation with the current analytical method of HPLC.

Moreover, the results obtained from the experiments with N-carbon catalyst revealed an interesting research path of the future. Besides the low reaction rate, this catalyst without any gold content is active for this oxidation reaction. From an economic viewpoint, this is an improvement which should be evaluated in future.

Once the impact of internal diffusion on this reaction is revealed and the data give an idea about the reaction in a future continuous process, the next step should be to investigate this sugar oxidation process in a continuous reactor system. One of the challenges is the control of the pH, because it is a very important parameter in the oxidation and in a continuous process it is not as easy to maintain a constant pH [46].

8. REFERENCES

[1] A.R. Morais, R. Bogel-Lukasik, Green chemistry and the biorefinery concept, Sustain Chem Process. 1 (2013) 18. https://doi.org/10.1186/2043-7129-1-18.

[2] A.T. Ubando, C.B. Felix, W.-H. Chen, Biorefineries in circular bioeconomy: A comprehensive review, Bioresource Technology. 299 (2020) 122585. https://doi.org/10.1016/j.biortech.2019.122585.

[3] A.J. Ragauskas, G.T. Beckham, M.J. Biddy, R. Chandra, F. Chen, M.F. Davis, B.H. Davison, R.A. Dixon, P. Gilna, M. Keller, P. Langan, A.K. Naskar, J.N. Saddler, T.J. Tschaplinski, G.A. Tuskan, C.E. Wyman, Lignin Valorization: Improving Lignin Processing in the Biorefinery, Science. 344 (2014) 1246843. https://doi.org/10.1126/science.1246843.

[4] H.K. Sharma, C. Xu, W. Qin, Biological Pretreatment of Lignocellulosic Biomass for Biofuels and Bioproducts: An Overview, Waste Biomass Valor. 10 (2019) 235–251. https://doi.org/10.1007/s12649-017-0059-y.

[5] B. Kamm, M. Kamm, P.R. Gruber, S. Kromus, Biorefinery Systems – An Overview, in: Biorefineries-Industrial Processes and Products, John Wiley & Sons, Ltd, 2008: pp. 1–40. https://doi.org/10.1002/9783527619849.ch1.

[6] D.Yu. Murzin, I.L. Simakova, 7.21 - Catalysis in Biomass Processing, in: J. Reedijk, K. Poeppelmeier (Eds.), Comprehensive Inorganic Chemistry II (Second Edition), Elsevier, Amsterdam, 2013: pp. 559–586. https://doi.org/10.1016/B978-0-08-097774-4.00727-0.

[7] B.T. Kusema, G. Hilpmann, P. Mäki-Arvela, S. Willför, B. Holmbom, T. Salmi, D.Yu. Murzin, Selective Hydrolysis of Arabinogalactan into Arabinose and Galactose Over Heterogeneous Catalysts, Catal Lett. 141 (2011) 408–412. https://doi.org/10.1007/s10562-010-0530-x.

[8] Approved additives and E numbers, Food Standards Agency. (n.d.). https://www.food.gov.uk/business-guidance/approved-additives-and-e-numbers (accessed May 10, 2020).

[9] D-Gluconic acid, American Chemical Society. (n.d.). https://www.acs.org/content/acs/en/molecule-of-the-week/archive/g/d-gluconic-acid.html (accessed May 10, 2020).

[10] Recovering rare earths from fertilizer waste, Chemical & Engineering News. (n.d.). https://cen.acs.org/materials/inorganic-chemistry/Recovering-rare-earths-fertilizer-waste/97/i10 (accessed May 10, 2020).

[11] Organic Synthesis with Carbohydrates | Wiley, Wiley.Com. (n.d.). https://www.wiley.com/en-us/Organic+Synthesis+with+Carbohydrates-p-9781850759133 (accessed May 25, 2020).

[12] R.V. Stick, Carbohydrates: The Sweet Molecules of Life, Elsevier, 2001.

[13] J.F. Robyt, Essentials of Carbohydrate Chemistry, Springer Science & Business Media, 2012.

[14] Aldoses - an overview | ScienceDirect Topics, (n.d.). https://www.sciencedirect.com/topics/biochemistry-genetics-and-molecular-biology/aldoses (accessed May 25, 2020).

[15] C. Fehér, Novel approaches for biotechnological production and application of L-arabinose, Journal of Carbohydrate Chemistry. 37 (2018) 251–284. https://doi.org/10.1080/07328303.2018.1491049.

[16] D.Y. Murzin, E.V. Murzina, A. Aho, M.A. Kazakova, A.G. Selyutin, D. Kubicka, V.L. Kuznetsov, I.L. Simakova, Aldose to ketose interconversion: galactose and arabinose isomerization over heterogeneous catalysts, Catal. Sci. Technol. 7 (2017) 5321–5331. https://doi.org/10.1039/C7CY00281E.
[17] S.B. Bankar, M.V. Bule, R.S. Singhal, L. Ananthanarayan, Glucose oxidase — An overview, Biotechnology Advances. 27 (2009) 489–501. https://doi.org/10.1016/j.biotechadv.2009.04.003.
[18] L.S. Correia, H. Grénman, J. Wärnå, T. Salmi, D.Yu. Murzin, Catalytic oxidation kinetics of arabinose on supported gold nanoparticles, Chemical Engineering Journal. 370 (2019) 952–961. https://doi.org/10.1016/j.cej.2019.03.241.
[19] B. T. Kusema, J.-P. Mikkola, D. Yu. Murzin, Kinetics of L-arabinose oxidation over supported gold catalysts with in situ catalyst electrical potential measurements, Catalysis Science & Technology. 2 (2012) 423–431. https://doi.org/10.1039/C1CY00365H.
[20] A. Corma, S. Iborra, A. Velty, Chemical Routes for the Transformation of Biomass into Chemicals, Chem. Rev. 107 (2007) 2411–2502. https://doi.org/10.1021/cr050989d.
[21] A. Corma, M.E. Domine, Gold supported on a mesoporous CeO2 matrix as an efficient catalyst in the selective aerobic oxidation of aldehydes in the liquid phase, Chem. Commun. (2005) 4042–4044. https://doi.org/10.1039/B506685A.
[22] C. Baatz, N. Decker, U. Prüße, New innovative gold catalysts prepared by an improved incipient wetness method, Journal of Catalysis. 258 (2008) 165–169. https://doi.org/10.1016/j.jcat.2008.06.008.
[23] B.T. Kusema, B.C. Campo, P. Mäki-Arvela, T. Salmi, D.Yu. Murzin, Selective catalytic oxidation of arabinose—A comparison of gold and palladium catalysts, Applied Catalysis A: General. 386 (2010) 101–108. https://doi.org/10.1016/j.apcata.2010.07.037.
[24] A.Yu. Klyushin, R. Arrigo, Y. Youngmi, Z. Xie, M. Hävecker, A.V. Bukhtiyarov, I.P. Prosvirin, V.I. Bukhtiyarov, A. Knop-Gericke, R. Schlögl, Are Au Nanoparticles on Oxygen-Free Supports Catalytically Active?, Top Catal. 59 (2016) 469–477. https://doi.org/10.1007/s11244-015-0528-0.
[25] SpinChem | Transforming your solutions, (n.d.). http://www.spinchem.com/ (accessed May 10, 2020).
[26] S. Franz, Aerobic oxidation of arabinose-glucose mixtures over gold nanoparticles., Master's Thesis. (2020). Laboratory of Industrial chemistry and Reaction Engineering. Faculty os Science and Engineering. Åbo Akademi University. Turku (Finland).
[27] E. Behravesh, N. Kumar, Q. Balme, J. Roine, J. Salonen, A. Schukarev, J.-P. Mikkola, M. Peurla, A. Aho, K. Eränen, D.Yu. Murzin, T. Salmi, Synthesis and characterization of Au nano particles supported catalysts for partial oxidation of ethanol: Influence of solution pH, Au nanoparticle size, support structure and acidity, Journal of Catalysis. 353 (2017) 223–238. https://doi.org/10.1016/j.jcat.2017.07.014.
[28] S. Biella, L. Prati, M. Rossi, Selective Oxidation of D-Glucose on Gold Catalyst, Journal of Catalysis. 206 (2002) 242–247. https://doi.org/10.1006/jcat.2001.3497.
[29] I. Sádaba, M.L. Granados, A. Riisager, E. Taarning, Deactivation of solid catalysts in liquid media: the case of leaching of active sites in biomass conversion reactions, Green Chem. 17 (2015) 4133–4145. https://doi.org/10.1039/C5GC00804B.

[30] W. Xing, M. Yin, Q. Lv, Y. Hu, C. Liu, J. Zhang, 1 - Oxygen Solubility, Diffusion Coefficient, and Solution Viscosity, in: W. Xing, G. Yin, J. Zhang (Eds.), Rotating Electrode Methods and Oxygen Reduction Electrocatalysts, Elsevier, Amsterdam, 2014: pp. 1–31. https://doi.org/10.1016/B978-0-444-63278-4.00001-X.

[31] D. Tromans, Temperature and pressure dependent solubility of oxygen in water: a thermodynamic analysis, Hydrometallurgy. 48 (1998) 327–342. https://doi.org/10.1016/S0304-386X(98)00007-3.

[32] Johan Warna, Cesar A. de Araujo Filho, Jose Rafael Hernandez Carucci,, Tapio Salmi, Chemical Reaction Engineering: A Computer-Aided Approach / Edition 1|Paperback, Barnes & Noble. (n.d.). https://www.barnesandnoble.com/w/chemical-reaction-engineering-tapio-salmi/1133899942?ean=9783110611458 (accessed June 15, 2020).

[33] J.B. Butt, Mass transfer in heterogeneous catalysis, C. N. Satterfield, Massachusetts Institute of Technology Press, Cambridge, Mass. (1970). 267 pages, AIChE Journal. 16 (1970) 509–510. https://doi.org/10.1002/aic.690160303.

[34] A. Burghardt, A. Kubaczka, Generalization of the effectiveness factor for any shape of a catalyst pellet, Chemical Engineering and Processing: Process Intensification. 35 (1996) 65–74. https://doi.org/10.1016/0255-2701(95)04115-X.

[35] R. Krishna, J.A. Wesselingh, The Maxwell-Stefan approach to mass transfer, Chemical Engineering Science. 52 (1997) 861–911. https://doi.org/10.1016/S0009-2509(96)00458-7.

[36] Principles and Modern Applications of Mass Transfer Operations, 3rd Edition | Wiley, Wiley.Com. (n.d.). https://www.wiley.com/en-us/Principles+and+Modern+Applications+of+Mass+Transfer+Operations%2C+3rd+Edition-p-9781119042730 (accessed June 1, 2020).

[37] C.J. Geankoplis, PROCESOS DE TRANSPORTE Y OPERACIONES UNITARIAS, CONTINENTAL, 1998.

[38] P. Fott, P. Schneider, Mass transport and a complex reaction in porous catalyst pellets: Thiophene hydrodesulphurization, Chemical Engineering Science. 39 (1984) 643–650. https://doi.org/10.1016/0009-2509(84)80171-2.

[39] T. Salmi, J. Wärmå, Modelling of catalytic packed-bed reactors—comparison of different diffusion models, Computers & Chemical Engineering. 15 (1991) 715–727. https://doi.org/10.1016/0098-1354(91)85017-O.

[40] R.C. Reid, J.M. Prausnitz, B.E. Poling, The properties of gases and liquids, (1987). https://www.osti.gov/biblio/6504847 (accessed May 7, 2020).

[41] D.F. Fairbanks, C.R. Wilke, Diffusion Coefficients in Multicomponent Gas Mixtures, Ind. Eng. Chem. 42 (1950) 471–475. https://doi.org/10.1021/ie50483a022.

[42] C.R. Wilke, P. Chang, Correlation of diffusion coefficients in dilute solutions, AIChE Journal. 1 (1955) 264–270. https://doi.org/10.1002/aic.690010222.

[43] R.E. Treybal, Treybal, Mass-transfer Operations, McGraw-Hill, 1980.

[44] X. Gao, M.R. Bonilla, J.C.D. da Costa, S.K. Bhatia, The transport of gases in macroporous α-alumina supports, Journal of Membrane Science. 409–410 (2012) 24–33. https://doi.org/10.1016/j.memsci.2012.03.003.

[45] S. Kolitcheff, E. Jolimaitre, A. Hugon, J. Verstraete, P.-L. Carrette, M. Tayakout-Fayolle, Tortuosity of mesoporous alumina catalyst supports: Influence of the pore network organization, Microporous and Mesoporous Materials. 248 (2017) 91–98. https://doi.org/10.1016/j.micromeso.2017.04.010.

[46] S. Saeid, Destruction of selected pharmaceuticals by ozonation and heterogeneous catalysis, (2020). Åbo Akademi - Åbo Akademi University https://www.doria.fi/handle/10024/176540 (accessed June 4, 2020).

APPENDIX I: MALVERN PLOTS DISTRIBUTION

- Small crushed catalyst

RESULTS		
Dv 10	Dv 50	Dv 90
69.1	175	371

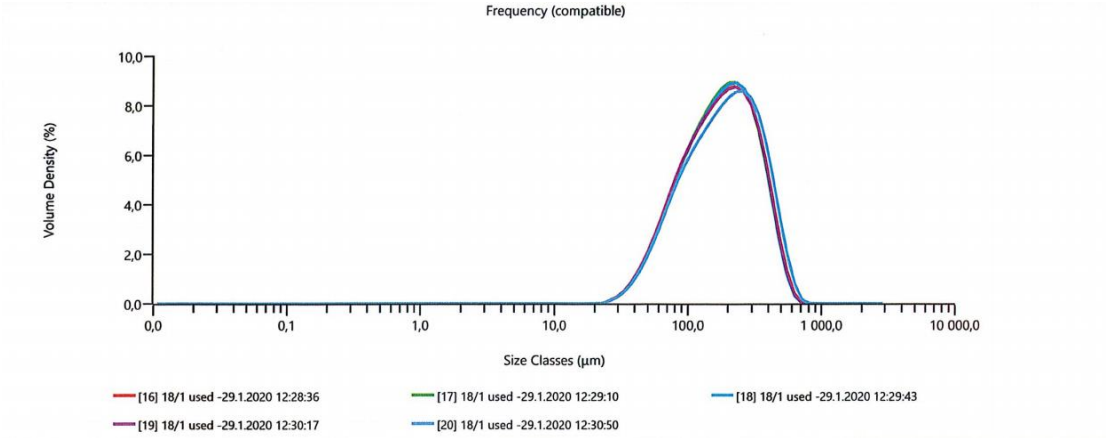

- Big crushed catalyst

RESULTS		
Dv 10	Dv 50	Dv 90
167	383	732

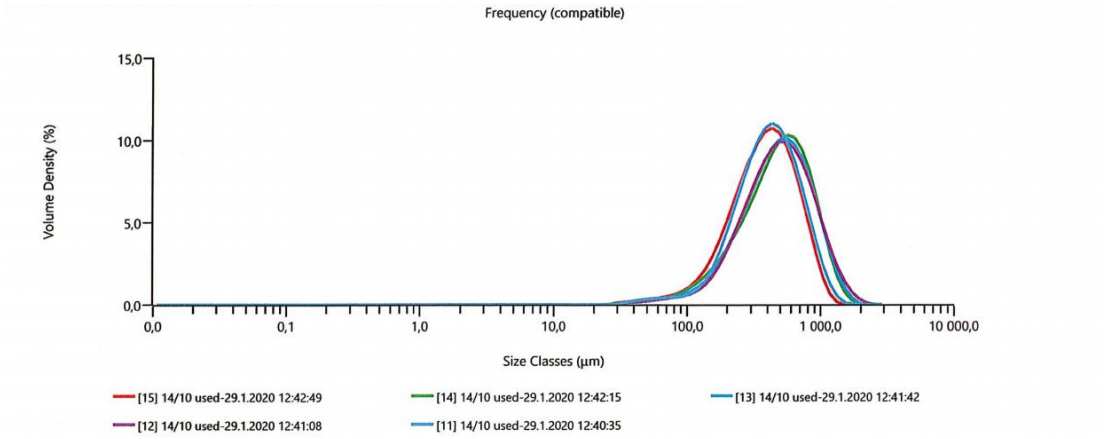

APPENDIX II: CHANGES IN ACID SUGARS RESIDENCE TIMES ON THE HPLC

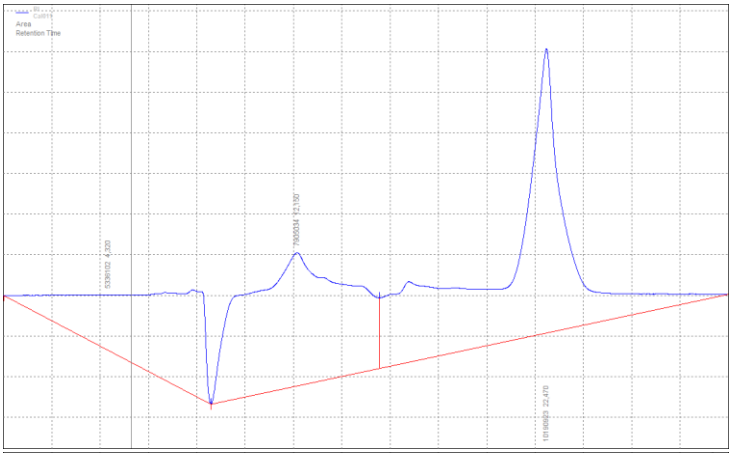

Time : 22,4

0,00375 g/ml

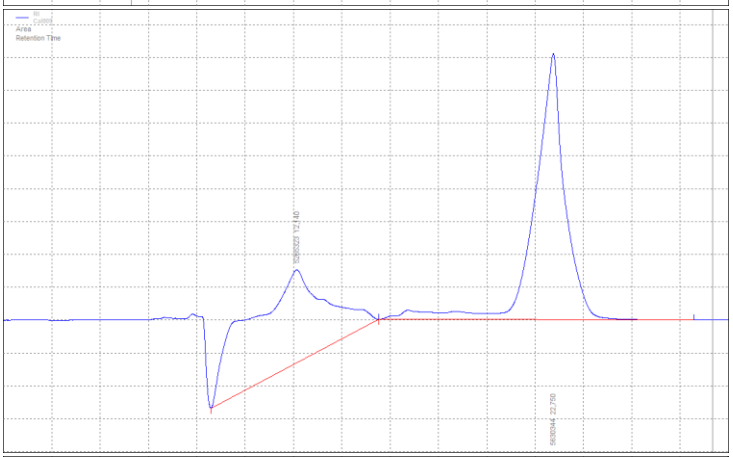

Time : 22,7

0,00625 g/ml

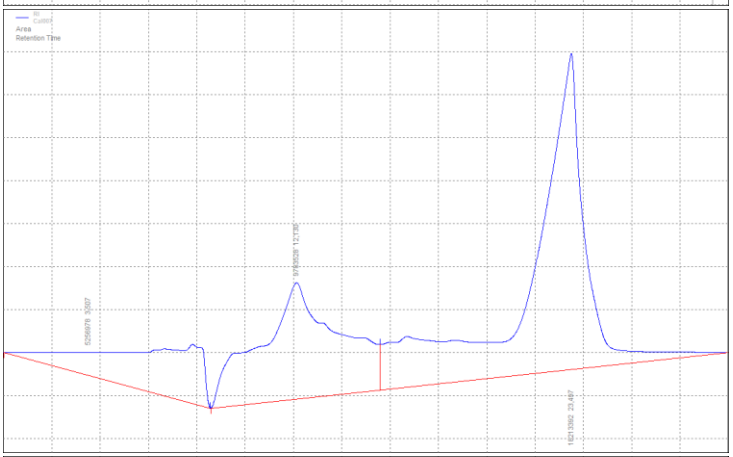

Time : 23,0

0,0083 g/ml

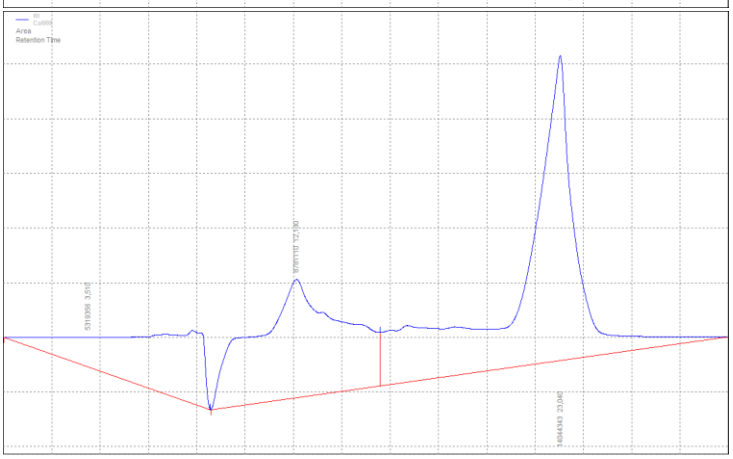

Time : 23,5

0,0125g/ml

During the analysis, it was observe a change in the residence time of the sugar acids, both of them, gluconic acid and arabinonic acid. to discard that this movement was due to the overlapping of different peaks coming from different compounds, the calibration was performed using only arabinonic acid. AS it is showed in the pictures, the calibration goes from 22.4 to 23.5.

APPENDIX III: KINETIC MODELING

```
clc, clear,
close all;
load DATA.mat;
%% Data
T = 343.15;             % Temperatura en K
RR = 8.314 ;            % constante de los gases ideales J(kg/m2s2)/molK
% inicial
Co = 0.103 ;            % mol/m3 maximun of oxygen dissolve in water
% initial concentratio of each experiemnte [Glu Ara]
C1_ini = [70.84, 72.94];
C2_ini = [96.075, 48.923];
C3_ini = [46.20, 95.62];
V =0.000150 ;               % m3
mcat = 1;           % g
dens = mcat*0.01/V;           % g Au/m3

%% Datos cineticos

K1 = 224.125716910677  ;          %Glu+O2 -> GlucO"     mol m3 min g Au
K2 =  717.641833218709  ;          %Ara+O2 -> AraO"
K3 =  4.16704999525874 ;       %Glu+O2 -> GluRO"
K4 = 0.607497321734236  ;           %Glu+O2 -> Fruct"
K5 =  7.34964377963257e-05 ;          %Glu+O2 -> Ribu"
KO  =  162.569443708546;
KGlu =  29.3569327599385 ;
KAra =  1610.11072226474;

%% Theoritical curve

Ks = [ K1, K2, K3, K4, K5, KO, KGlu, KAra];
% N es el numeor de moles concetracion*V
% Experiment 1
N1_ini = zeros(8,1);
N1_ini(1)= C1_ini(1)*V;
N1_ini(2)= Co*V;
N1_ini(3)= C1_ini(2)*V;
% Experiment 2
N2_ini = zeros(8,1);
N2_ini(1)= C2_ini(1)*V;
N2_ini(2)= Co*V;
N2_ini(3)= C2_ini(2)*V;
% Experiment 3
N3_ini = zeros(8,1);
N3_ini(1)= C3_ini(1)*V;
N3_ini(2)= Co*V;
N3_ini(3)= C3_ini(2)*V;

t_int = [0,3500]; %(min)

equation  = @(t,N)odefit(t,N,Ks,dens,V,Co);
[t,N1] = ode15s(equation,t_int,N1_ini);

figure(1)
for i = 1:8
plot(t, N1/V/1000);
hold on
end
```

```
ylabel('mol of compound');
xlabel('time (min)');
legend('Glucose','Oxygen','Arabinose','GluO','AraO','GluRO')

%% fitting

Rx =-1*eye(8);
b = zeros(8,1);

Kss = fmincon(@fcoste,Ks,Rx,b)

equation  = @(t,N)odefit(t,N,Kss,dens,V,Co);
[tt1,Ni1] = ode15s(equation,DATA050220(:,1),N1_ini);
[tt2,Ni2] = ode15s(equation,DATA170220(:,1),N2_ini);
[tt3,Ni3] = ode15s(equation,DATA200220(:,1),N3_ini);

for i=1:25
V1=150;
    A1(i,:) = Ni1(i,:)/V1*1000;
end
GluO_Rib = A1(:,8)+A1(:,4);
Ara_Fruc = A1(:,7)+A1(:,3);
Matrix = zeros(25,5);
Matrix(:,1) = A1(:,1);
Matrix(:,2) = Ara_Fruc;
Matrix(:,3) = A1(:,5);
Matrix(:,4) = GluO_Rib;
Matrix(:,5) = A1(:,6);

for i=1:18
    V2(i)= (interp1(VOL170220(:,1),VOL170220(:,2),tt2(i)))-1*i;
    A2(i,:) = Ni2(i,:)/V2(i)*1000;
end
GluO_Rib2 = A2(:,8)+A2(:,4);
Ara_Fruc2 = A2(:,7)+A2(:,3);
Matrix2 = zeros(18,5);
Matrix2(:,1) = A2(:,1);
Matrix2(:,2) = Ara_Fruc2;
Matrix2(:,3) = A2(:,5);
Matrix2(:,4) = GluO_Rib2;
Matrix2(:,5) = A2(:,6);

for i=1:18
    V3(i)= (interp1(VOL200220(:,1),VOL200220(:,2),tt3(i)))-1*i;
    A3(i,:) = Ni3(i,:)/V3(i)*1000;
end
GluO_Rib3 = A3(:,8)+A3(:,4);
Ara_Fruc3 = A3(:,7)+A3(:,3);
Matrix3 = zeros(18,4);
Matrix3(:,1) = A3(:,1);
Matrix3(:,2) = Ara_Fruc3;
Matrix3(:,3) = A3(:,5);
Matrix3(:,4) = GluO_Rib3;


figure (3)
hold on
plot(DATA050220(:,1),DATA050220(:,2),'ob','MarkerSize',3)
plot(DATA050220(:,1),DATA050220(:,3),'or','MarkerSize',3)
plot(DATA050220(:,1),DATA050220(:,4),'om','MarkerSize',3)
```

```
plot(DATA050220(:,1),DATA050220(:,5),'oc','MarkerSize',3)

plot(tt1, Matrix(:,1),'b');
plot(tt1, Matrix(:,2),'r');
plot(tt1, Matrix(:,3),'m');
plot(tt1, Matrix(:,4),'c');

hold off

title('050220')
xlabel('time (min)');
ylabel('concentration (mol/L)');
legend('Glucose','Ara + Fruc','GluO + Rib','AraO')

figure (4)
hold on
plot(DATA170220(:,1),DATA170220(:,2),'ob','MarkerSize',3)
plot(DATA170220(:,1),DATA170220(:,3),'or','MarkerSize',3)
plot(DATA170220(:,1),DATA170220(:,4),'om','MarkerSize',3)
plot(DATA170220(:,1),DATA170220(:,5),'oc','MarkerSize',3)
plot(DATA170220(:,1),DATA170220(:,6),'og','MarkerSize',3)

plot(tt2, Matrix2(:,1),'b');
plot(tt2, Matrix2(:,2),'r');
plot(tt2, Matrix2(:,3),'m');
plot(tt2, Matrix2(:,4),'c');
plot(tt2, Matrix2(:,5),'g');

hold off

title('170220')
xlabel('time (min)');
ylabel('concentration (mol/L)');
legend('Glucose','Ara + Fruc','GluO + Rib','AraO')


figure (5)
hold on
plot(DATA200220(:,1),DATA200220(:,2),'ob','MarkerSize',3)
plot(DATA200220(:,1),DATA200220(:,3),'or','MarkerSize',3)
plot(DATA200220(:,1),DATA200220(:,4),'om','MarkerSize',3)
plot(DATA200220(:,1),DATA200220(:,5),'oc','MarkerSize',3)


plot(tt3, Matrix3(:,1),'b');
plot(tt3, Matrix3(:,2),'r');
plot(tt3, Matrix3(:,3),'m');
plot(tt3, Matrix3(:,4),'c');

hold off

title('200220')
xlabel('time (min)');
ylabel('concentration (mol/L)');
legend('Glucose','Ara + Fruc','GluO + Rib','AraO')
```

ODEFIT

```
function dN = odefit(t,N,Ks,dens,V,Co)

    K1 = Ks(1);
    K2 = Ks(2);
    K3 = Ks(3);
    K4 = Ks(4);
    K5 = Ks(5);
    KO = Ks(6);
    KGlu = Ks(7);
    KAra = Ks(8);

    dN =zeros(8,1);
    N(2)= Co;
    %Concentraciones
    xGlu = N(1)/V;
    xo = N(2)/V;
    xAra = N(3)/V;
    xGluO = N(4)/V;
    xAraO = N(5)/V;
    xGluRO = N(6)/V;
    xFruc = N(7)/V;
    xRib = N(8)/V;

    r1 = K1*xGlu*xo/(1+KGlu*xGlu+KAra*xAra+KO*xo)^2;
    r2 = K2*xAra*xo/(1+KGlu*xGlu+KAra*xAra+KO*xo)^2;
    r3 = K3*xGlu*xo/(1+KGlu*xGlu+KAra*xAra+KO*xo)^2;
    r4 = K4*xGlu/(1+KGlu*xGlu+KAra*xAra+KO*xo);
    r5 = K5*xAra/(1+KGlu*xGlu+KAra*xAra+KO*xo);


    rGlu = -(r1+r3+r4);
    ro = -(r1+r2+r3);
    rAra = -(r2+r5);
    rGluO = r1;
    rAraO = r2;
    rGluRO = r3;
    rFruc = r4;
    rRib = r5;

    dN(1) = rGlu*(dens*V);
    dN(2) = 0;
    dN(3) = rAra*(dens*V);
    dN(4) = rGluO*(dens*V);
    dN(5) = rAraO*(dens*V);
    dN(6) = rGluRO*(dens*V);
    dN(7) = rFruc*(dens*V);
    dN(8) = rRib*(dens*V);


end
```

FCOST

```
function Diff = fcoste(Ks)

    load('DATA.mat')

    % DATA

    V =0.000150 ;               % m3
    mcat = 1;           % g
    dens = mcat*0.01/V;           % g Au/m3
    Co = 0.103 ;            % mol/m3

    % initial concentration of each experiemnte [Glu Ara] mol/m3
    C1_ini = [70.84, 72.94];
    C2_ini = [96.075, 48.923];
    C3_ini = [46.20, 95.62];

    % Experiment 1
    N1_ini = zeros(8,1);    %mol
    N1_ini(1)= C1_ini(1)*V;
    N1_ini(2)= Co*V;
    N1_ini(3)= C1_ini(2)*V;
    % Experiment 2
    N2_ini = zeros(8,1);
    N2_ini(1)= C2_ini(1)*V;
    N2_ini(2)= Co*V;
    N2_ini(3)= C2_ini(2)*V;
    % Experiment 3
    N3_ini = zeros(8,1);
    N3_ini(1)= C3_ini(1)*V;
    N3_ini(2)= Co*V;
    N3_ini(3)= C3_ini(2)*V;


    %Resolucion de ODE
    equation2  = @(t,N)odefit(t,N,Ks,dens,V,Co);
    [tt1,Ni1] = ode15s(equation2,DATA050220(:,1),N1_ini);
    [tt2,Ni2] = ode15s(equation2,DATA170220(:,1),N2_ini);
    [tt3,Ni3] = ode15s(equation2,DATA200220(:,1),N3_ini);
    for i=1:25
        V1(i)= (interp1(VOL050220(:,1),VOL050220(:,2),tt1(i)))-1*i; % mL
        A1(i,:) = Ni1(i,:)/V1(i)*1000;          %mol/L
    end
    GluO_Rib = A1(:,8)+A1(:,4);
    Ara_Fruc = A1(:,7)+A1(:,3);
    Matrix = zeros(25,5);
    Matrix(:,1) = A1(:,1);
    Matrix(:,2) = Ara_Fruc;
    Matrix(:,3) = A1(:,5);
    Matrix(:,4) = GluO_Rib;
    Matrix(:,5) = A1(:,6);
%
    for i=1:18
        V2(i)= (interp1(VOL170220(:,1),VOL170220(:,2),tt2(i)))-1*i;
        A2(i,:) = Ni2(i,:)/V2(i)*1000;
    end
```

```
GluO_Rib2 = A2(:,8)+A2(:,4);
Ara_Fruc2 = A2(:,7)+A2(:,3);
Matrix2 = zeros(18,5);
Matrix2(:,1) = A2(:,1);
Matrix2(:,2) = Ara_Fruc2;
Matrix2(:,3) = A2(:,5);
Matrix2(:,4) = GluO_Rib2;
Matrix2(:,5) = A2(:,6);

for i=1:18
    V3(i)= (interp1(VOL200220(:,1),VOL200220(:,2),tt3(i)))-1*i;
    A3(i,:) = Ni3(i,:)/V3(i)*1000;
end
GluO_Rib3 = A3(:,8)+A3(:,4);
Ara_Fruc3 = A3(:,7)+A3(:,3);
Matrix3 = zeros(18,4);
Matrix3(:,1) = A3(:,1);
Matrix3(:,2) = Ara_Fruc3;
Matrix3(:,3) = A3(:,5);
Matrix3(:,4) = GluO_Rib3;

%funcion de coste
Dif1 = (DATA050220(:,[2,3,4,5,6])-Matrix).^2;
Dif2 = (DATA170220(:,[2,3,4,5,6])-Matrix2).^2;
Dif3 = (DATA200220(:,[2,3,4,5])-Matrix3).^2;
S1Dif = sum(Dif1);
S2Dif = sum(Dif2);
S3Dif = sum(Dif3);
S11Dif = sum(S1Dif);
S22Dif = sum(S2Dif);
S33Dif = sum(S3Dif);

Diff = (S11Dif + S22Dif + S33Dif)

end
```

APPENDIX IV: CALIBRATION CURVES

0,6 ml/min		RSQ	SLOPE	INTERCEPT
g/100ml	area			
Arabinose		0.998795	1.04E-07	-0.01041
1.001	9538167			
0.5005	5083945			
0.25025	2498199			
0.125125	1241156			
0.062563	626937			
0.031281	309413			
D-Arabinoic acid		0.999647	7.76E-08	0.017568
0.96	12112014			
0.48	6168451			
0.24	2986419			
0.12	1347142			
0.06	612389			
0.03	132077			
D-Arabino-y-lactone		0.993301	8.78E-08	-0.00565
0.1	1222032			
0.05	594042.6			
0.025	313076.1			
0.0125	221771.3			
0.00625	175473.7			

		RSQ	SLOPE	INTERCEPT
g/100ml	area			
Glucose		0.998059	1E-07	-0.01581
1.001	9985368			
0.5005	5424184			
0.25025	2663970			
0.125125	1344712			
0.062563	686336			
0.031281	342045			
Gluconic acid		0.997006	8.15E-08	-0.0314
2.070	25644730			
1.035	12800747			
0.518	7774024			
0.259	3457447			
0.129	1723761			
0.065	905343			
Glucuronic acid		0.999648	7E-08	0.028846
1	13790500			
0.5	6895075			
0.25	3188202			
0.125	1300779			
0.0625	440074			
Fructose		0.99993	9.86E-08	0.004814
1	6080750			
0.5	5017173			
0.25	2509506			
0.125	1202803			
0.0625	587311			